Reaction Mechanisms and Thermochemistry of $V^+ + C_2H_{2p}$ ($p = 1-3$)

N. Aristov and P. B. Armentrout*†

Contribution from the Department of Chemistry, University of California, Berkeley, California 94720. *Received August 26, 1985*

Abstract: The reactions of ground-state vanadium ions with ethane, ethene, and ethyne have been studied by using the guided ion beam technique. Reactions with cross sections as small as 10^{-4} Å^2 are examined in detail. This allows observation of not only the primary products but also species corresponding to the rearrangement and decomposition of these products. The predominant process in all systems is symmetric cleavage of the carbon–carbon bond to form VCH_p^+. The second most probable reaction is formation of vanadium hydride ion. The only low energy products observed are $VC_2H_4^+$ and $VC_2H_2^+$, from dehydrogenation of ethane and ethene, respectively. Modeling of the translational energy dependence of endothermic reactions yields bond energies for the ions V^+–CH_r and V^+–C_2H_r ($r = 0-3$). This thermochemistry is used to help identify product structures and reaction mechanisms.

Interactions of transition metals with hydrocarbons are of importance in biochemical processes, organometallic chemistry, C–H bond activation, and homo- and heterogeneous catalysis. Detailed mechanistic and thermodynamic data on such interactions, however, are only currently becoming available. In developing a fuller picture of the fundamental processes involved in metal chemistry, various mass spectrometric techniques have been particularly useful. Reactivity of atomic metal ions with organic molecules has been studied by using both ion beam mass spectrometry[1] and ICR (ion cyclotron resonance; FTMS).[2-6] These gas-phase methods are valuable because they allow the interactions between a metal ion and a hydrocarbon to be probed in the absence of other potentially influential effects such as the solvent and ligand sphere. Unlike ICR, the beam technique has the additional ability to examine endothermic reaction channels. Thus, it provides a systematic means for measuring thermodynamic data for such systems.

In this paper, we report results of ion beam studies of reactions of atomic vanadium ions with C_2 hydrocarbons: ethane, ethene, and ethyne.[7] Previous beam studies have looked extensively at ethene and ethane chemistry, although this earlier work focused on determining the thermochemistry of only the major processes—hydrogen abstraction and carbon–carbon bond cleavage. Results include data for Cr^+, Mn^+, Fe^+, Co^+, and Ni^+.[1] More recently, the C–C bond cleavage reactions of ethane with Sc^+ [8] and the second-row metals, Ru^+, Rh^+, and Pd^+ [9] have been studied. The chemistry of ethyne with bare transition-metal ions has not been noted in the literature, but FeO^+ has been shown to be reactive toward C_2H_2 at thermal energies.[5a] In the present work, a comprehensive examination of all reactions in the three C_2 systems is made. Detailed data for the threshold regions of all endothermic product channels are obtained. These are interpreted to yield a set of self-consistent bond energies between V^+ and CH_r and C_2H_r ($r = 0-3$). A summary of this thermochemistry and its implications for the electronic structure of these species has been presented in brief.[10] The results presented here have been only slightly revised and updated.

The data reported here are some of the first results obtained by using a guided ion beam apparatus of unique design. By incorporating an octopole ion trap in the interaction region, the apparatus avoids many of the problems inherent in conventional ion beam instruments. Experiments can be performed from very high energies (hundreds of eV) to near thermal energies (as low as 0.05 eV, lab). For the first time, beam results can be directly compared with data from ICR or flowing afterglow experiments. In addition, collection efficiency is improved to the point that product ion losses due to dynamic effects are small. Consequently, the sensitivity of the apparatus is extremely high. This permits observation of processes with cross sections as small as 10^{-4} Å^2 and provides a detailed view of the threshold regions for endothermic product channels. An excellent opportunity is offered for the evaluation of a variety of theoretical threshold models, resulting in improved reliability in the quantitative determination of the reaction endothermicities and derived thermochemical values. Our ability to examine thresholds of even minor reaction channels allows the derivation of thermochemistry from several independent reactions. This provides an internal check of the measured bond energies. This procedure, which has not heretofore been possible, avoids misinterpretation of the thresholds due to activation barriers and kinetic shifts.

Experimental Section

General. A schematic diagram of the ion beam instrument is presented in Figure 1. A complete description of the apparatus and analysis of its capabilities is given elsewhere.[11] The apparatus comprises three differentially pumped vacuum chambers. In the source chamber, ions are produced in one of several interchangeable modules. Ions are extracted from the source, accelerated, and focused onto the entrance slit of a magnetic mass spectrometer.[12] The mass-selected ions enter the second vacuum chamber where they are refocused and decelerated to a desired kinetic energy by using an exponential retarding lens.[13] At this

† Presidential Young Investigator, 1984–1989.

(1) (a) Armentrout, P. B.; Beauchamp, J. L. *J. Chem. Phys.* **1981**, *74*, 2819. (b) *J. Am. Chem. Soc.* **1981**, *103*, 784–791. (c) *Ibid.* **1981**, *103*, 6628–6632. (d) Armentrout, P. B.; Halle, L. F.; Beauchamp, J. L. *Ibid.* **1981**, *103*, 6624–6628. (e) *Ibid.* **1981**, *103*, 6501–6502. (f) Halle, L. F.; Armentrout, P. B.; Beauchamp, J. L. *Organometallics* **1982**, *1*, 963–968. (g) *Ibid.* **1983**, *2*, 1829–1833. (h) Halle, L. F.; Crowe, W. E.; Armentrout, P. B.; Beauchamp, J. L. *Ibid.* **1984**, *3*, 1694–1706.

(2) (a) Burnier, R. C.; Byrd, G. D.; Freiser, B. S. *J. Am. Chem. Soc.* **1981**, *103*, 4360–4367. (b) Byrd, G. D.; Burnier, R. C.; Freiser, B. S. *Ibid.* **1982**, *104*, 3565–3569. (c) Byrd, G. D.; Freiser, B. S. *Ibid.* **1982**, *104*, 5944–5950. Jacobson, D. B.; Freiser, B. S. *Ibid.* **1983**, *105*, 5197–5206.

(3) Allison, J.; Ridge, D. P. *J. Am. Chem. Soc.* **1977**, *99*, 35–39; **1978**, *100*, 163. Allison, J.; Freas, R. B.; Ridge, D. P. *Ibid.* **1979**, *101*, 1332. Allison, J.; Ridge, D. P. *Ibid.* **1979**, *101*, 4998. Freas, R. B.; Ridge, D. P. *Ibid.* **1980**, *102*, 7129–7131. Larsen, Barbara S.; Ridge, D. P.; *Ibid.* **1984**, *106*, 1912–1922.

(4) Radecki, B. D.; Allison, J. *J. Am. Chem. Soc.* **1984**, *106*, 946. Cassady, C. J.; Freiser, B. S.; McElvany, S. W.; Allison, J. *Ibid.* **1984**, *106*, 6125. Babinec, S. J.; Allison, J. *Ibid.* **1984**, 106, 7718.

(5) (a) Kappes, M. M.; Staley, R. H. *J. Am. Chem. Soc.* **1981**, *103*, 1286–1287. (b) *Ibid.* **1982**, *104*, 1813–1819. Jones, R. W.; Staley, R. H. *J. Phys. Chem.* **1982**, *86*, 1387–1392, 1669–1674. *J. Am. Chem. Soc.* **1980**, *102*, 3794–3798. Uppal, J. S.; Staley, R. H. *Ibid.* **1980**, *102*, 4144.

(6) (a) Foster, M. S.; Beauchamp, J. L. *J. Am. Chem. Soc.* **1975**, *97*, 4808. (b) Halle, L. F.; Houriet, R.; Kappes, M. M.; Staley, R. H.; Beauchamp, J. L. *Ibid.* **1982**, *104*, 6293.

(7) In unpublished work, both Freiser and Kappes noted no reactions between V^+ and C_2's at thermal energies. (Freiser, B. S., private communication. Kappes, M. M. Ph.D. Thesis, M.I.T., 1981.)

(8) Tolbert, M. A.; Beauchamp, J. L. *J. Am. Chem. Soc.* **1984**, *106*, 8117–8122.

(9) Mandich, M. L.; Halle, L. F.; Beauchamp, J. L. *J. Am. Chem. Soc.* **1984**, *106*, 4403–4411.

(10) Aristov, N.; Armentrout, P. B. *J. Am. Chem. Soc.* **1984**, *106*, 4065–4066.

(11) Ervin, K. M.; Armentrout, P. B. *J. Chem. Phys.* **1985**, *83*, 166–189.

(12) Gentry, W. R. LRL Report UCRL-17691, 1967.

0002-7863/86/1508-1806$01.50/0

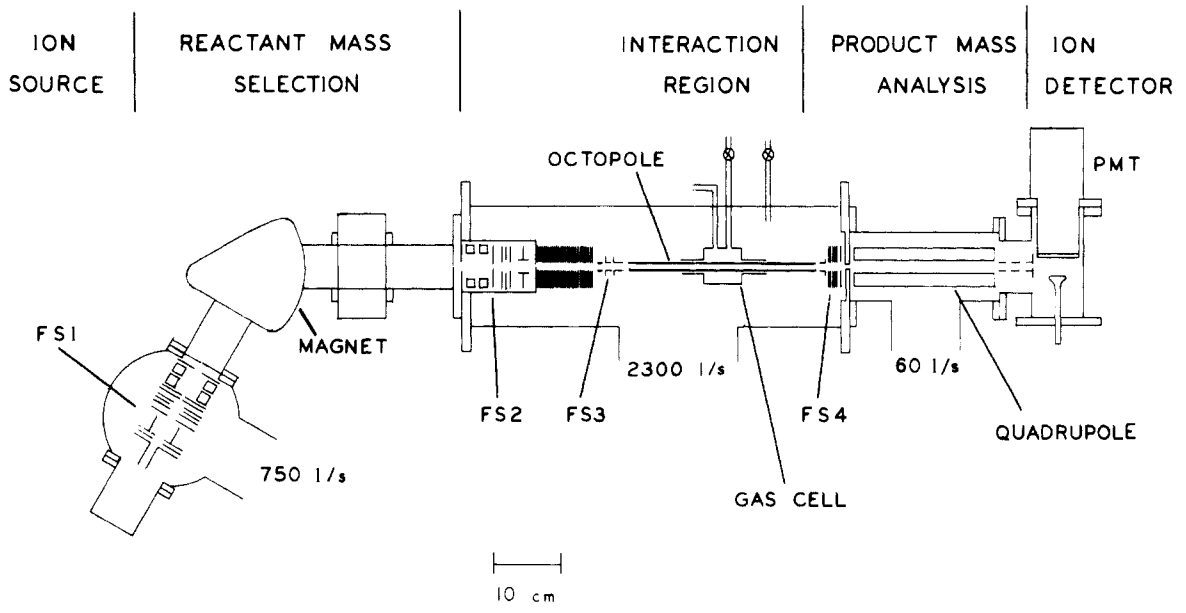

Figure 1. Schematic of the guided ion beam tandem mass spectrometer.

point, the ions are injected into an octopole ion trap.[14] Radio frequency electric fields establish a radial potential well which traps ions over a broad mass range. The velocity of the ions parallel to the axis of the trap is not affected.

The octopole trap passes through a static gas cell into which a reactant gas can be introduced. Pressures of the gas are monitored by a capacitance manometer (MKS Baratron Model 170) and are maintained at a sufficiently low level, 0.10–0.50 mtorr, that multiple collisions of the ions with the gas are improbable. Unreacted beam and product ions are contained in the trap until they drift out of the cell and to the end of the trap. Here, dc ion optics extract the ions and focus them into the detector chamber where they are analyzed by a quadrupole mass filter. Mass-analyzed ions are detected with a scintillation ion detector[15] and processed by pulse-counting techniques. Experiments are fully automated with a DEC MINC computer which collects the ion signals as it sweeps the product masses and incident ion energy.

The total reaction cross section, σ, is calculated from the data by using eq 1, where n is the number density of the neutral gas, l is the effective gas cell length, I is the measured intensity of the transmitted ion beam,

$$\sigma = -\ln (I/I_0)nl \tag{1}$$

and I_0 is the sum of the intensities of all ions, $I + \sum I_i$, where the subscript i refers to a specific product channel. Experiments have demonstrated that product ion collection efficiencies are high and that under our operating conditions, mass discrimination effects, in the octopole trap and in the quadrupole mass filter, are small.[11] I_0, therefore, is very nearly equal to the incident ion intensity. Cross sections for individual product ions, σ_i, are calculated by using expression 2.

$$\sigma_i = \sigma I_i / \sum_i I_i \tag{2}$$

Accuracies of the reported cross sections are limited primarily by our ability to measure the target gas density and to estimate the effective gas cell length.[16] Absolute cross sections are estimated to have an uncertainty of ±20% and are in good agreement with literature data on well-characterized systems.[11] Uncertainties in cross section values near zero (for example, in the vicinity of the threshold for an endothermic product channel) can be much larger. This is primarily due to random counting noise (typically, 5 counts/s). Reactions which occur outside the collision cell and overlap of neighboring mass peaks may also add to the background signal. All these contributions are determined by introducing the reactant gas directly into the second vacuum chamber rather than into the gas cell on alternate mass–energy sweeps. Subtraction of this background from the signal obtained with gas in the gas cell yields, I_i, the intensity of ions produced inside the cell. Random scatter in the data results in some negative values for cross sections near zero.

Table I. Distribution of V^+ Electronic States at 1800, 1925, and 2200 K, and Average Electronic Energy in the V^+ Beam[a]

		filament temp, K		
state	E_{el}[b]	1800	1925	2200
^5D	0.026	0.861	0.843	0.806
^5F	0.363	0.138	0.156	0.191
^3F	1.104	<0.001	0.0011	0.0023
^3P	1.452	≪0.001	≪0.001	<0.001
^3H	1.566			<0.001
^3F	1.681			<0.001
^5P	1.692			≪0.001
fraction ($\times 10^3$)[c]		0.8 (±0.2)	1.3 (±0.2)	3.0 (±0.2)
E_{el}, eV[d]		0.073	0.079	0.094

[a] Electronic states and energy levels are from ref 42. [b] Energies are averaged over the J levels. [c] Fraction of states having energies exceeding 1 eV. [d] Average electronic energy of the V^+ beam at the specified temperature.

Ion Source. Vanadium ions are produced by using surface ionization of $VOCl_3$ (Aesar, 99.995%; used as received, except for multiple freeze–pump–thaw cycles). The source comprises a resistively heated rhenium filament (20 × 0.05 × 0.76 mm) surrounded by a U-shaped repeller. The center of the filament and the repeller are held at the same potential—the nominal zero energy of the ions. The filament is exposed to $VOCl_3$ vapor which enters from a glass tube located to the side of the filament and repeller.

These studies were performed at three filament temperatures, 1800, 1925, and 2200 ± 50 K, which were calibrated in a test stand using optical pyrometry. Table I shows the fraction of electronic states in the V^+ beam at the given filament temperature, assuming a Maxwell–Boltzmann distribution. The resulting average electronic energy in the beam has no more than a 2.5-meV uncertainty due to the 50 K uncertainty in the filament temperature.

The flight time of the ions from the source to the interaction region is approximately 50–150 μs. The lifetimes of the electronically excited species are experimentally unknown. They are expected to be seconds or greater, well in excess of the flight time, as all transitions between the states listed in Table I are parity forbidden.[17] Consequently, we assume that the beam has the state population calculated in the table.

Energy Scale. Laboratory energies (lab) are related to the center of mass (CM) energies by using the simple relationship

$$E_{CM} = E_{lab} m/(M + m) \tag{3}$$

where M and m are the masses of the incident ion and neutral reactant, respectively. The vanadium isotope at 50.944 amu (99.75%, natural

(13) Vestal, M. L.; Blakely, C. R.; Ryan, P. W.; Futrell, J. H. *Rev. Sci. Instrum.* **1976**, *47*, 15.
(14) Teloy, E.; Gerlich, D. *Chem. Phys.* **1974**, *4*, 417. (b) Frobin, W.; Schlier, Ch.; Strein, K.; Teloy, E. *J. Chem. Phys.* **1977**, *67*, 5505.
(15) Daly, N. R. *Rev. Sci. Instrum.* **1960**, *31*, 264.
(16) The effective gas cell length is corrected for end effects. The nominally 12 cm long cell has an effective length of 8.6 cm. The validity of this correction is experimentally verified by measuring the magnitude of processes with known cross sections.[11] The effective cell length is believed to be accurate to ±10%.
(17) Elkind, J. L.; Armentrout, P. B. *J. Phys. Chem.* **1985**, *89*, 5626–5636.

abundance) was used exclusively in these studies. To measure the absolute energy scale, the octopole is used as a high-efficiency retarding field analyzer (RFA). Because the retarding region and interaction region are physically the same, this energy measurement has no uncertainties due to space charge, contact potentials, or focusing aberrations. By scanning through the nominal ion energy zero (determined by the potential difference between the ion source filament and the dc voltage on the octopole), we obtain a nearly ideal "cutoff" curve. The differential of this curve with respect to energy is represented well by a Gaussian peak. The center of this peak is taken to be the true zero of the ion energy (E_0), and its width characterizes the ion beam's kinetic energy distribution. In these studies, the true zero is found to be offset from the nominal zero by as much as 0.7 eV lab (0.25 eV CM, calculated for ethene). The full width at half-maximum (fwhm) of the ion distribution is independent of energy and is commonly 0.6 eV lab (0.20 eV CM for ethyne, 0.21 eV CM for ethene, and 0.22 eV CM for ethane). The behavior of the octopole as an RFA has been verified by using time-of-flight measurements.[11] Contributions from transverse energies have been shown to be negligible. Absolute uncertainties in the energy scale are less than ±0.1 eV lab (<0.04 eV CM).

While the ion beam energy spread contributes some uncertainty to the energy scale, a larger effect is the thermal motion of the neutral gas.[18] This distribution, referred to as Doppler broadening, has a width in the center of mass frame of $0.46E^{1/2}$ eV for ethyne, $0.45E^{1/2}$ for ethene, and $0.44E^{1/2}$ eV for ethane. In comparing theoretical cross sections with the data, the calculated cross sections must be convoluted with the experimental energy distribution. Both sources of broadening are included in our convolution using formulas given by Lifschitz et al.[19]

Theoretical Section

Low Energy. The energy dependence of bimolecular rearrangements

$$A^+ + BCD \rightarrow ABC^+ + D - \Delta E \quad (4)$$

is an area of much discussion. Exothermic ion molecule reactions ($\Delta E < 0$) are often described by using the Langevin–Gioumousis–Stevenson[20] (LGS) form of the cross section

$$\sigma_L = \pi e(2\alpha/E)^{1/2} \quad (5)$$

where e is the unit of charge, α is the polarizability of the neutral molecule, and E is the relative translational energy of the reactants. This form is derived from the long-range ion-induced dipole potential and assumes the absence of chemical activation barriers. Equation 5 is often a reliable upper limit for exothermic ion–molecule reactions (assuming the neutral has no dipole moment) but is rarely in detailed quantitative agreement with experimental results.[11,21] Typical magnitudes of exothermic cross sections at thermal energies are 10–100 Å^2. For reactions with ethane, ethene, and ethyne where α = 4.39, 4.10, and 3.04 Å^3,[22] respectively, σ_L at 1 eV is 35.3, 34.1, and 29.4 Å^2.

While observation of an exothermic reaction does imply a lower limit for the ABC^+ bond dissociation energy, $D°(A^+–BC) > D°(BC–D)$, endothermic processes ($\Delta E > 0$) are potentially more useful in learning the thermodynamics of a system. Assuming there is no activation energy in excess of the endothermicity, a knowledge of BCD's thermochemistry and an accurate measurement of ΔE can yield the bond strength of ABC^+. Theory and experiment indicate that excitation functions in the threshold region can be parametrized by using eq 6,[1,23] where σ_0 is an energy-in-

$$\sigma(E) = \sigma_0(E - \Delta E)^n/E^m \quad (6)$$

dependent scaling factor having units of Å^2 eV$^{(m-n)}$, E is the total energy available to the reactants, and ΔE is the reaction endothermicity. In these studies, E is given to a good approximation by the relative translational energy of the reactants. Thus, if n and m were known for a particular reaction system, evaluation of ΔE would be straightforward. We have tried to use available theory as a guide in choosing physically realistic values of n and m. Unfortunately, theory is rather divided in its predictions as can be demonstrated by examining the assortment of values predicted for n and m in the simplest case, an *atom–diatom* reaction.

Morokuma et al.[24] use collision theory to derive an expression for tight transition states and find that m = 3 and n = 4 or 3.5, depending on whether the transition state is linear or nonlinear. It is straightforward to show that for loose transition states, n should equal 3. Chesnavich and Bowers[25] found that for reactions that are translationally pumped, m = 1 and n is dependent on the transition-state geometry. For a linear activated complex, n = 2, while for a nonlinear species n = 1.5. A loose transition state yields n = 1, which is the same form as the line of centers model.[23] Use of the stationary phase approximation yields a form for a direct process where n = 2.5 and m = 1.5.[26] Phase space theory predicts n = 1.25 and m = 0.[27] Nonstatistical methods of analysis, such as scattering theory, have predicted $n = m$ = 0.5.[28] Experimentalists have often used a linear form (n = 1, m = 0) for computational convenience.[14b,19,29] In previous beam studies of metal reactions,[1a] Armentrout and Beauchamp (AB) used the more general form given by eq 6 but limited themselves to forms where $n = m$ at integral or half-integral values. The value of n was determined from analysis of the high-energy falloff region of the cross section using eq 7. In this expression, D is the

$$\sigma(E) = \sigma_0[D/fE]^n \quad (7)$$

dissociation energy of the bond being ruptured in the neutral reactant, f is the average fraction of internal energy in the ionic product, and σ_0, n, and E are defined as in eq 6. If this equation describes the data, then a log–log plot of σ vs. E in the falloff region should give a line with a slope of $-n$. This value can then be plugged into eq 6 for determination of ΔE.[1a]

In this work, we have examined the applicability of a wide range of values for n and m. Based on the theories cited above, we have specifically evaluated cases where m = 0, 1, 1.5, 3, and n and allowed n to vary freely to best fit the data. In practice, threshold energies are determined by calculating a theoretical cross section using eq 6 with a set value of m, convoluting over the energy distribution, and then varying the parameters n, ΔE, and σ_0 until good agreement to the data is found. The best values are determined by using a nonlinear least-squares analysis based on programs by Bevington.[30] Generally, several sets of parameters fit the data equally well. However, despite large variations in n and m, ΔE values are usually restricted to a narrow range (<0.5 eV). Thus, the thermochemistry derived here is fairly insensitive to the parameters used to fit the data.

High Energy. Cross sections are observed to peak and then decrease when ABC^+ contains too much energy to remain a stable product or when a primary reaction channel (such as the formation of AD^+) becomes available and competes favorably with the production of ABC^+. In the first case, the peak of the cross section can occur in close proximity to the threshold of the process

$$A^+ + BCD \rightarrow ABC^+ + D \rightarrow A^+ + BC + D - \Delta E' \quad (8)$$

where $\Delta E'$ is just $D°(BC–D)$. The peak is shifted to higher energies if energy goes into the internal modes of the neutral product or preferentially into translation. If the peak of the cross section is at a value lower than $D°(BC–D)$, then either the ion is decomposing by a different low-energy pathway (e.g., $AB^+ + C$) or a competitive primary reaction channel has opened. By noting the correspondence between the peak of $\sigma(ABC^+)$ and the thresholds of other products (AB^+ or AD^+, for instance), it is possible to identify what process causes the production of this ion to decrease. (The exception is any dissociation which re-forms the reactant ion, e.g., process 8, since this product is obscured by the unreacted beam. Thus, process 8, an indirect collision induced dissociation (CID), is inferred by its effect on the cross section for production of the ABC^+ intermediate.) This allows a detailed reaction scheme to be developed by examining both the formation and dissociation energies of all the products.

Bond Energies. There are questions which remain concerning the conversion of threshold energies, ΔE, to thermochemical values of interest, $D°(A^+–BC)$. This conversion is made by using the relation

$$\Delta E = D°(BC–D) - D°(A^+–BC) - E_{el} \quad (9)$$

where E_{el} accounts for excited electronic states in the reactant beam. Possible problems with the accuracy of this conversion are analogous to those encountered in the determination of ionization and appearance

(18) Chantry, P. J. *J. Chem. Phys.* 1971, *55*, 2746.
(19) Lifschitz, C.; Wu, R. L. C.; Tiernan, T. O.; Terwilliger, D. T. *J. Chem. Phys.* **1978**, *68*, 247.
(20) Gioumousis, G.; Stevenson, D. P. *J. Chem. Phys.* **1958**, *29*, 294.
(21) Henchman, M. In "Ion–Molecule Reactions"; Franklin, J. L., Ed.; Plenum Press: New York, 1972; Vol. 1, p 101.
(22) Rothe, E. W.; Bernstein, R. B. *J. Chem. Phys.* **1959**, *31*, 1619.
(23) Levine, R. D.; Bernstein, R. B. "Molecular Reaction Dynamics"; Oxford: New York, 1974; Chapter 2.
(24) Morokuma, K.; Eu, B. C.; Karplus, M. *J. Chem. Phys.* **1969**, *51*, 5193.
(25) Chesnavich, W. J.; Bowers, M. T. *J. Phys. Chem.* **1979**, *83*, 900.
(26) Menzinger, M.; Yokozeki, A. *Chem. Phys.* **1977**, *22*, 273.
(27) Chesnavich, W. J.; Bowers, M. T. *J. Chem. Phys.* **1978**, *68*, 901.
(28) Eu, B. C.; Liu, W. S. *J. Chem. Phys.* **1975**, *63*, 592.
(29) Berkowitz, J.; Chupka, W. A.; Gutman, D. *J. Chem. Phys.* **1971**, *55*, 2733–2745.
(30) Bevington, P. R. "Data Reduction and Error Analysis for the Physical Sciences"; McGraw-Hill: New York, 1964.

Table II. Heats of Formation and Bond Dissociation Energies (kcal/mol)[a]

ion (VBC^+)	$\Delta H°_{298}(VBC^+)$	$D°$
V^{+b}	278.6 (2)	
V^+–H[c]	284 (2)	48 (1)
V^+–C	361 (1)	91 (1)
V^+–CH	307 (3)	114 (2)
VC^+–H	307 (3)	106 (3)
V^+–CH_2	296 (3)	76 (2)
VCH^+–H	296 (3)	63 (5)
V^+–CH_3	263 (3)	50 (2)
VCH_2^+–H	263 (3)	85 (5)
V^+–C_2	351 (5)	126 (4)[d]
VC^+–C	351 (5)	180 (5)[d]
V^+–C_2H	295 (3)	119 (2)
VC_2^+–H	295 (3)	108 (6)
VC^+–CH	295 (3)	207 (3)
V^+–C_2H_2	282 (5)	51 (5)
VC_2H^+–H	282 (5)	65 (6)
VCH^+–CH	282 (5)	167 (6)
V^+–C_2H_3	261 (6)	88 (5)[d]
$VC_2H_2^+$–H	261 (6)	73 (8)[d]
VCH^+–CH_2	261 (6)	140 (6)[d]
V^+–C_2H_4	~241	~50[e]

[a] Uncertainties are quoted in parentheses; 23.060 94 kcal/mol = 1.00 eV. [b] Calculated from the ionization potential of V given in ref 42 and ΔH_{298} of V_g from: Chase, M. W., et al. *J. Phys. Chem. Ref. Data* **1975**, *4*, 1. [c] Reference 36. [d] These bond energies are most conservatively viewed as lower limits. [e] Estimate. See text.

Table III. Heats of Formation Used in Deriving Experimental Results

neutral	$\Delta H°_{298}$, kcal/mol	neutral	$\Delta H°_{298}$, kcal/mol
H	52.1	C_2H	135.0 (1)[b]
C	171.3 (0.02)	C_2H_2	54.2 (0.2)
CH	142.3 (0.2)	C_2H_3	70.4 (2)[b]
CH_2	93.4 (0.2)	C_2H_4	12.5 (0.2)
CH_3	35.1 (0.2)[b]	C_2H_5	28.3 (1.1)[c]
CH_4	−17.9 (0.2)	C_2H_6	−20.2 (0.2)
C_2	198.8 (0.2)		

[a] All values, except where noted, are from: Wagman, D. D., et al. *J. Phys. Chem. Ref. Data* **1982**, *11*, Supp. 2. Uncertainties in parentheses. [b] Reference 37. [c] William von Eggers Doering, *Proc. Natl. Acad. U.S.A.* **1981**, *78*, 5279–5283.

potentials. For example, the possibility of kinetic shift effects[31] and activation barriers can lead to values of ΔE in excess of the endothermicity and, thus, low bond energies.

The influence of kinetic shifts is reduced by the sensitivity of our instrument which is on the order of 1 in 10^6. Processes with cross sections as small as 10^{-4} Å^2 can be detected. Thus, errors due to kinetic shifts are anticipated to be minimal. Activation barriers in ion–molecule chemistry are generally held to be negligible, due to the long-range ion-induced dipole attraction. Exothermic ion–molecule reactions are usually observed to proceed with large cross sections at low energies. (Counterexamples generally involve failure to conserve spin or angular momentum.[32]) In order to test for activation barriers, a given bond dissociation energy is measured by using several different reactions. Self-consistency among the derived values helps ensure that the correct thermochemistry is obtained. The test for self-consistency also helps avoid errors due to kinetic shift effects.

There is some ambiguity as to whether the internal temperature of the products *at threshold* is best characterized by a temperature of 300 K (the temperature of the gas cell and neutral reactant) or 0 K. Since we attempt to make no corrections for the energy available in the internal modes of the reactants, we assume that the values obtained are more characteristic of 300 K. This assumption should affect the thermochemistry by no more than 1 kcal/mol.

The presence of electronically excited states of V^+ is accounted for by using the average electronic excitation energy, 0.08 eV (1.8 kcal/mol) (see Table I). Detailed calculations taking explicit account of the individual microstates give similar thermochemical results. This correction implicitly assumes that all states have equal reactivity. In the absence of more detailed data, this is the only sensible assumption.

The major component of error in threshold values is due to the uncertainty in the theoretical parameters of eq 6. As noted above, many sets of parameters can usually be found which adequately represent the data. For each process, the bond energy is obtained by eq 9, using the *mean* threshold value calculated from ΔE's of the best fits for each m tested in eq 6. The thermochemistry in Table II is the average bond energy calculated from all the processes yielding a particular ion. The error limits are the standard deviation of these values plus the uncertainty of the hydrocarbon thermochemistry given in Table III. The parameters m, n, and ΔE of eq 6 for each reaction are listed in Table IV.

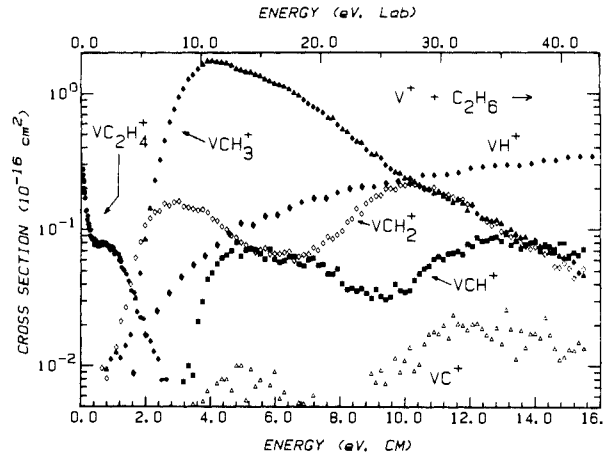

Figure 2. Variation of product cross sections with translational energy in the laboratory frame (upper axis) and the center-of-mass frame (lower axis) for reaction of V^+ and C_2H_6.

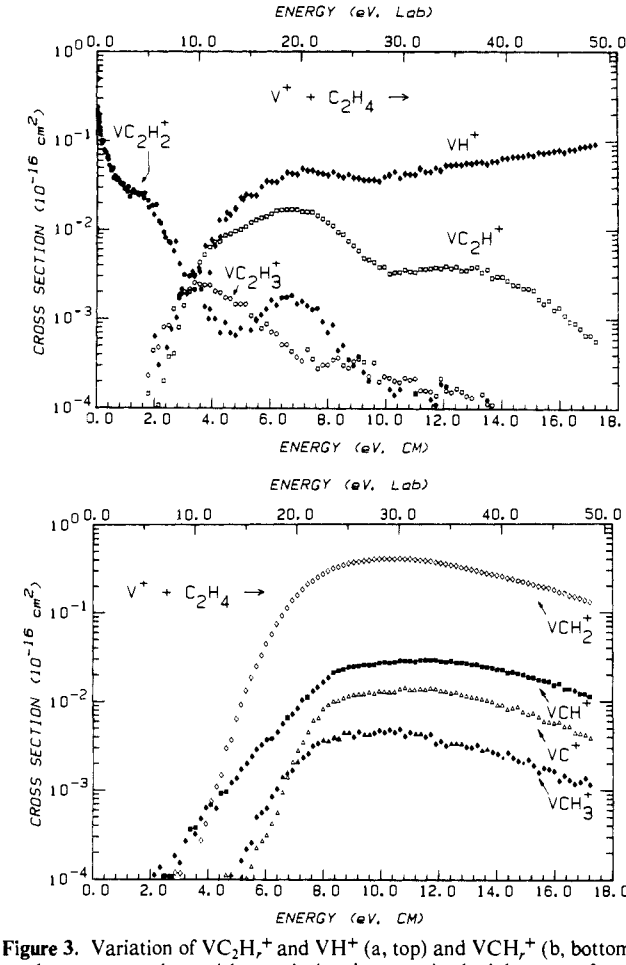

Figure 3. Variation of $VC_2H_r^+$ and VH^+ (a, top) and VCH_r^+ (b, bottom) product cross sections with translational energy in the laboratory frame (upper axis) and center-of-mass frame (lower axis) for reaction of V^+ and C_2H_4.

(31) Beynon, J. H.; Gilbert, J. R. In "Gas Phase Ion Chemistry"; Bowers, M. T., Ed.; Academic Press: New York, 1979; Vol. 2, Chapter 13, pp 166–168.

(32) Armentrout, P. B.; Halle, L. F.; Beauchamp, J. L. *J. Chem. Phys.* **1982**, *76*, 2449–2457. Armentrout, P. B.; Beauchamp, J. L. *Chem. Phys.* **1980**, *50*, 27–36.

Table IV. Parameters of Equation 6 Used in Fitting Threshold Regions[a]

ionic product	neutral reactant		m 0.0	1.0	1.5	3.0	n
VC^+	C_2H_2	n =	0.8	1.4	1.5	1.7	1.0
		ΔE =	9.66	9.37	9.35	9.32	9.58
	C_2H_4	n =	1.0	1.1	1.2	1.1	1.1
		ΔE =	6.90	6.88	6.86	6.97	6.87
	C_2H_6	n =		1.0			
		ΔE =		3.58			
VCH^+	C_2H_2	n =	3.3	3.7	4.0	4.7	6.9
		ΔE =	6.38	6.26	6.20	6.04	5.61
	C_2H_6	n =	1.2	1.4	2.6	3.0	1.6
		ΔE =	3.48	3.48	3.20	3.18	3.48
VCH_2^+	C_2H_4	n =	2.5	3.0	3.2	4.0	5.8
		ΔE =	4.51	4.41	4.36	4.21	3.85
	C_2H_6	n =	2.4	3.1	3.4	4.6	
		ΔE =	0.87	0.81	0.79	0.72	
VCH_3^+	C_2H_4	n =	1.6	1.9	2.1	2.7	2.5
		ΔE =	5.09	5.00	4.96	4.80	4.87
	C_2H_6	n =	1.7	2.2	2.5	3.4	4.1
		ΔE =	1.79	1.72	1.69	1.61	1.54
VC_2^+	C_2H_2	n =	2.9	3.4	3.7	4.5	
		ΔE =	5.40	5.27	5.21	5.03	
VC_2H^+	C_2H_2	n =	2.3	3.2	3.7	5.1	
		ΔE =	0.67	0.57	0.53	0.43	
	C_2H_4	n =	2.0	2.4	2.6	3.4	4.3
		ΔE =	2.43	2.38	2.35	2.26	2.11
$VC_2H_2^+$	C_2H_4	n =		2.0	2.5		
		ΔE =		4.20	3.91		
$VC_2H_3^+$	C_2H_4	n =	2.4	3.3	3.7	5.1	14.0
		ΔE =	1.11	0.99	0.93	0.80	0.60

[a] Blanks indicate that no acceptable fit was found.

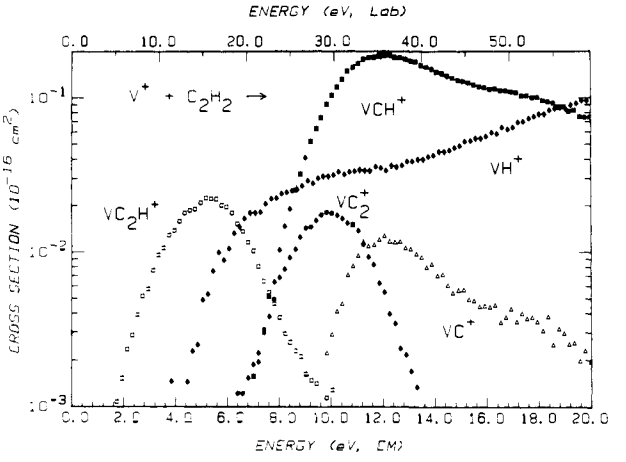

Figure 4. Variation of product cross sections with translational energy in the laboratory frame (upper axis) and center-of-mass frame (lower axis) for reaction of V^+ and C_2H_2.

Results and Discussion

Overview. Figures 2, 3, and 4 show the cross sections of all the products observed in ethane, ethene, and ethyne, respectively. The reaction channels observed for each system can be grouped into two major categories: C–C and C–H bond cleavage. The former process is favored at higher energies and results primarily in symmetric cleavage, i.e., production of VCH_p^+ from C_2H_{2p}. Rearrangement channels yielding $VCH_{p+1}^+ + CH_{p-1}$ or $VCH_{p-1}^+ + CH_{p+1}$ are observed in ethene ($VCH_3^+ + CH$ and $VCH^+ + CH_3$) and ethane ($VCH_2^+ + CH_4$). These pathways are not as favorable as the direct cleavage channel. At higher energies, these ionic products decompose primarily by breaking the metal–ligand bond but also by loss of H atoms and by elimination of H_2.

Cleavage of the hydrocarbon C–H bonds by vanadium ions results in several products. The lowest energy process in the case of ethane and ethene is dehydrogenation of the parent hydrocarbon to create $VC_2H_{2p-2}^+ + H_2$. In all systems, vanadium hydride ion is the major C–H cleavage product at elevated energies. Much smaller amounts of the competing product, $VC_2H_{2p-1}^+$, are formed in the ethene and ethyne systems. No $VC_2H_5^+$ is observed with ethane. Given that there are more C–H bonds than there are C–C bonds in ethane and ethene, it is interesting that VH^+ is *not* the major product in any system.

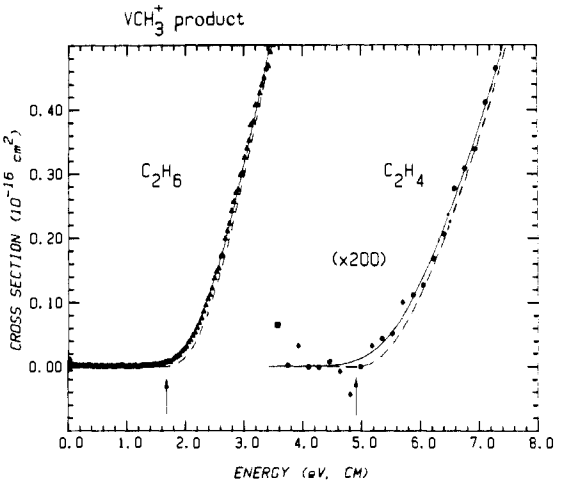

Figure 5. Threshold regions of $\sigma(VCH_3^+)$ seen in $V^+ + C_2H_6$ (▲) and $V^+ + C_2H_4$ (●). The solid lines are fits to the data convoluted with the energy broadening, as discussed in the text. The dashed lines are the same fits, unconvoluted. The arrows indicate the derived threshold energies.

Product ions that did not contain vanadium were not observed. This is presumably due to the much lower ionization potentials of vanadium-containing species than of the hydrocarbons. In cases where the ionization potential of the metal complex is high (e.g., $ZnCH_3$[33]) or that of the hydrocarbon low (e.g., t-C_4H_9),[34] such hydrocarbon ions are easily observed with our instrument.

It should be noted that these experiments have no *direct* way of detecting neutral products or determining ion structure. Identification of the former is usually unambiguous once the reaction energetics are considered. In the following discussion, only the reactions forming VH^+ have substantial uncertainty in the neutral product identification, and this is true only at high energies. Elucidation of the ions' structure can be achieved by examining their thermochemistry and decomposition products. The latter method is equivalent to collision-induced dissociation studies of ion structure, with the experimental limitation that the decomposition pathway may be obscured by other reaction channels.

A detailed analysis of all reaction channels is contained in the following sections. The threshold regions grouped according to the product ion are shown in Figures 5–10. The best $m = n$ fits, unconvoluted and convoluted over the ion beam and Doppler broadening, are also shown and discussed below. As was stated in the theoretical section, n and m are often perceived to be related to the number of active degrees of freedom in the transition state. In these experiments, we find that these parameters are similar for a given *ionic product*, irrespective of the reaction by which it was formed.

The models for atom–diatom reactions presented in the Theoretical section are directly applicable to only a few of the reactions observed here. This is not surprising, given the complexity of these systems. Despite the lack of a good threshold theory, the thermochemistry derived from these endothermic cross-section curves is relatively insensitive to the models used. In addition, agreement between V^+–R bond energies obtained from several reactions is quite good. As a result, the thermochemistry listed in Table II is believed to be free of systematic errors.

Thresholds. 1. Vanadium Methyl Ion. The production of VCH_3^+ from the reaction of V^+ and ethane (Figure 5) rises steeply from an apparent threshold near 1.5 eV. The fits to these data

(33) Georgiadis, R.; Armentrout, P. B. *J. Am. Chem. Soc.*, in press.
(34) Elkind, J. L.; Aristov, N.; Georgiadis, R.; Sunderlin, L.; Armentrout, P. B., unpublished results.

yield a mean threshold of 1.67 ± 0.10 eV. The lowest energy reaction producing VCH_3^+ is simple C–C cleavage, eq 10. Using

$$V^+ + C_2H_6 \rightarrow VCH_3^+ + CH_3 \quad (10)$$

eq 9 and $D°(H_3C–CH_3)$ = 3.92 eV from Table III, we calculate a $V^+–CH_3$ bond energy of 2.17 ± 0.10 eV (50 ± 2 kcal/mol). In all systems discussed below, bond energies are derived from threshold energies in a similar manner. This process is the only *major* reaction channel of all three systems to which we can apply one of the direct atom–diatom models [n = 2, m = 1;[25] n = 2.5, m = 1.5[26]] discussed above. This may indicate that the internal modes of methyl are relatively inactive and do not contribute appreciably to the reaction dynamics. A similar conclusion was drawn in an analysis of the reaction K + CH_3I → KI + CH_3 where n = 2.5 and m = 1.5 were used.[26]

Halle et al. observed reactions analogous to process 10 with Fe^+, Co^+, and Ni^+.[1d] The fits used to model $\sigma(MCH_3^+)$ in their data were $m = n$ = 3 for Fe^+ and $m = n$ = 5 for Co^+ and Ni^+ using a method of modeling put forth in the Theoretical section. As originally derived by Armentrout and Beauchamp (AB),[1a,b] this model is applicable only to species which have only one decomposition pathway. It can be clearly seen in Figure 2 that the falloff region of $\sigma(VCH_3^+)$ contains two distinct sections with different slopes. These begin near 4 and 6.5 eV. This suggests that vanadium methyl ion primarily dissociates via reaction 11, starting at $D°(H_3C–CH_3)$ = 3.92 eV. Near 6.5 eV, a second

$$V^+ + C_2H_6 \rightarrow VCH_3^+ + CH_3 \rightarrow V^+ + 2CH_3 \quad (11)$$

dissociation pathway (loss of an H atom, discussed below) begins. Strictly speaking, the AB model should be applied to the section of the falloff where *only* reaction 11 is occurring, between 4 and 6.5 eV. A log–log plot of the data in this region yields a line with a slope such that n = 1.1. Use of this value in eq 6 ($n = m$) yields a fit which fails to reproduce the data and gives a high threshold of 2.24 eV. If the model is applied to the secondary decomposition region above 6.5 eV, we derive n = 3.5. Using this n in eq 6, we obtain ΔE = 1.58 eV. These parameters are not too different from those obtained by our optimization method, which yields $n = m$ = 4.1 and ΔE = 1.54 eV (Table IV). Our conclusion is that while the *exclusive* use of $n = m$ is probably not justified, it can yield reliable thermochemical data. The use of the high-energy falloff region to identify the best value of n and m, however, is probably inappropriate. The theoretical justification for this procedure is not borne out by the present data.

VCH_3^+ is also formed in reaction with ethene, process 12. The threshold value of 4.94 ± 0.11 eV leads to $D°(V^+–CH_3)$ = 2.13 ± 0.11 eV in excellent agreement with the ethane result. This

$$V^+ + C_2H_4 \rightarrow VCH_3^+ + CH \quad (12)$$

is encouraging, considering that formation of VCH_3^+ is a very minor reaction channel (Figure 3b) and must involve a complex mechanism. The values of n (for a given m) for this cross section are close to those used in the ethane system. That such similar functions should describe both a simple methyl transfer and a complex rearrangement demonstrates that these parameters should not be overinterpreted.

The recommended bond strength of $V^+–CH_3$ given in Table II is the average of the results obtained from ethane and ethene, 2.15 ± 0.10 eV (50 ± 2 kcal/mol). Table V contains a compilation of other first-row transition-metal ion–methyl bond energies. Our value for $D°(V^+–CH_3)$ is quite consistent with these and fits well within the general downward trend of the values for the left side of the periodic table. The general periodic trend observed in these values is typical for many physical properties of the transition-metal series.[35]

2. Vanadium Carbene Ion. Figure 6 shows the threshold regions of $\sigma(VCH_2^+)$ seen in reactions with ethene and ethane. In the former system, reaction 13, the cross section rises slowly. As a

$$V^+ + C_2H_4 \rightarrow VCH_2^+ + CH_2 \quad (13)$$

(35) Cotton, F. A.; Wilkinson, Geoffrey "Advanced Inorganic Chemistry", 3rd ed.; Wiley-Interscience: New York, 1972.

Table V. First-Row Transition-Metal Ion Bond Energies

M	$D(M^+–CH_3)^a$	$D(M^+–CH_2)^a$
Sc	59 (5), 65 (5)[c]	97 (6)
Ti	56 (5)	85 (6)
V	50 (2)[b]	76 (2)[b]
Cr	30 (5), 37 (7)[d]	52 (3), 65 (7)[d]
Mn	51 (5), 71 (7)[d]	94 (7)[d]
Fe	64 (5), 69 (4)[e]	96 (5),[d] 82 (5)[f]
Co	61 (4)[d]	85 (7),[d] 84 (5)[f]
Ni	49 (5), 48 (5)[d]	86 (6)[d]

[a] All values, in kcal/mol, are from ref 34 except as noted. Uncertainties in parentheses. [b] This work. [c] Reference 8. [d] Reference 1e. [e] Reference 1f. [f] Hettich, R. L.; Freiser, B. S. *J. Am. Chem. Soc.*, submitted.

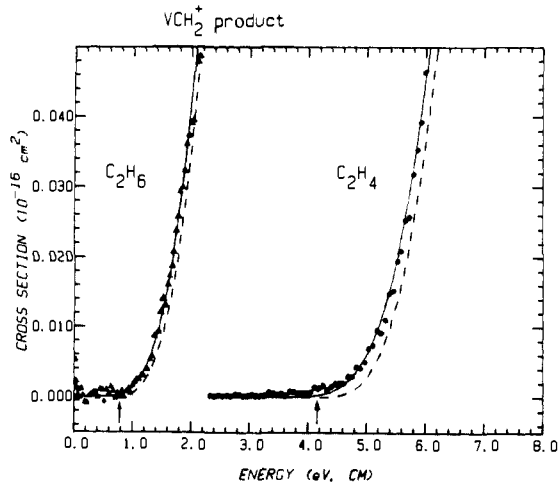

Figure 6. Threshold regions of $\sigma(VCH_2^+)$ seen in $V^+ + C_2H_6$ (▲) and $V^+ + C_2H_4$ (●). The solid lines are calculated fits, convoluted over the energy broadening. The dashed lines are the same fits, without the convolution. Arrows indicate the derived thresholds.

consequence, higher values of n are necessary to fit these data than were used to fit the VCH_3^+ cross sections. For instance, the best $m = n$ fit is n = 5.8 and ΔE = 3.85 eV. The average ΔE value is 4.17 ± 0.11 eV, leading to a $V^+–CH_2$ bond energy of 3.32 ± 0.11 eV.

The only other detailed study of a process similar to eq 13 was done by Armentrout and Beauchamp with cobalt ions.[1a] Using their method of analysis (AB), they derive $n = m$ = 5, but also find good fits to the data with $n = m$ = 4 or 6. While the best $n = m$ value derived here is similar, the AB method is difficult to apply to the V^+ data since the falloff region is nonlinear on a log–log scale. The best fit above 12 eV yields n = 2.5, a fairly low value. Using this in eq 6 gives ΔE = 4.97 eV, which is beyond the error limits of our best fits. In future work, it will be interesting to see if reactions of other metal ions with C_2H_4 have energy dependences more like V^+ or Co^+.

In the ethane system, the threshold of the vanadium carbene ion is 0.79 ± 0.06 eV for fits using m = 0, 1, 1.5, and 3. No good $n = m$ fits were found. The calculated fit in Figure 6 for this threshold is the m = 3 result. If reaction 14 is responsible for this product ion, then the bond energy for $V^+–CH_2$ is 3.28 ± 0.06 eV, in good agreement with that obtained from C_2H_4.

$$V^+ + C_2H_6 \rightarrow VCH_2^+ + CH_4 \quad (14)$$

In the ethane system, VCH_2^+ is also formed as a decomposition product of VCH_3^+, reaction 15. This can be seen in Figure 2 as the second peak in the VCH_2^+ cross section beginning above 6.5 eV. This accounts for the break in the falloff of the VCH_3^+ cross

$$V^+ + C_2H_6 \rightarrow VCH_3^+ + CH_3 \rightarrow VCH_2^+ + H + CH_3 \quad (15)$$

section discussed above. The predicted threshold for reaction 15, based on the thermochemistry derived above, is 5.4 eV. Modeling of this high-energy feature is imprecise because of overlap between the falloff of reaction 14 with the threshold of reaction 15.

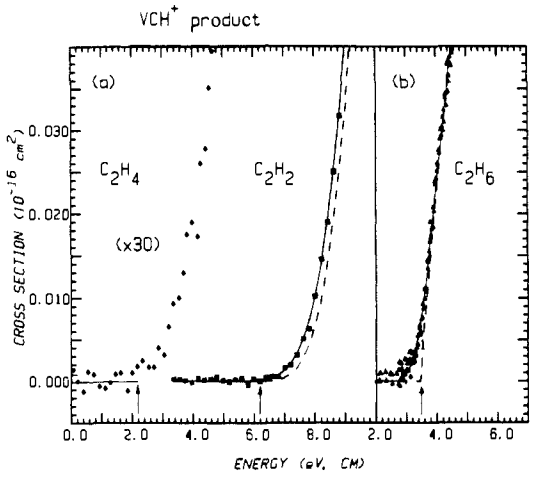

Figure 7. Threshold regions of $\sigma(VCH^+)$ observed in reactions of (a) $V^+ + C_2H_4$ (●), $V^+ + C_2H_2$ (■), and (b) $V^+ + C_2H_6$ (▲). The solid lines are calculated fits convoluted over the energy broadening. The dashed lines are the same fits, with no convolution. Note that the x-axis energy scale is not continuous. Arrows indicate the derived thresholds.

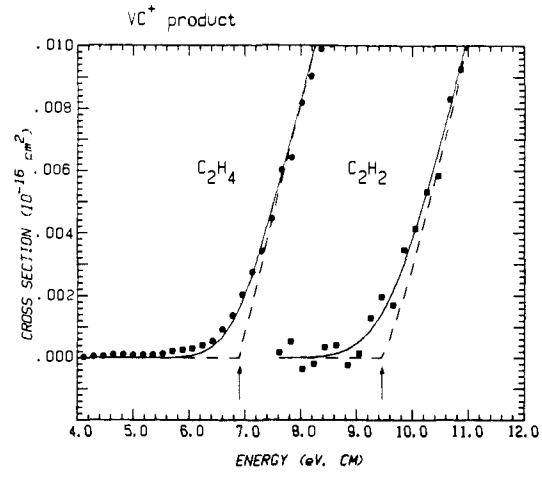

Figure 8. Threshold regions of $\sigma(VC^+)$ seen in $V^+ + C_2H_4$ (●) and $V^+ + C_2H_2$ (■). The solid lines through the points are calculated fits, convoluted over the energy broadening. The dashed lines are the same fits with no convolution. Arrows indicate the derived threshold energies.

However, a change of slope in $\sigma(VCH_2^+)$ is indicated at the predicted thermodynamic limit.

Our value of $D°(V^+–CH_2) = 3.30 \pm 0.06$ eV (76 ± 2 kcal/mol) is taken from the average of the results of reactions 13 and 14. Other metal ion–carbene bond energies are listed in Table V. The $V^+–CH_2$ bond strength measured here is consistent with these and fits within the downward trend of the left-side $M^+–CH_2$ bond strengths.

3. Vanadium Carbyne Ion. Production of VCH^+ is seen in all three reaction systems (Figure 7). The VCH^+ cross section from ethyne, like $\sigma(VCH_2^+)$ in the C_2H_4 system, rises slowly. The best fits have an average threshold of 6.20 ± 0.10 eV. Reaction 16 gives a $V^+–CH$ bond energy of 3.71 ± 0.10 eV. If a logarithmic

$$V^+ + C_2H_2 \rightarrow VCH^+ + CH \quad (16)$$

fit is made above 12 eV to the falloff of the cross section (Figure 4), then the AB method of analysis yields $n = m = 1.8$ and $\Delta E = 7.80$ eV. This is very different from our optimized $n = m$ threshold fit of $n = 6.9$ and $\Delta E = 5.61$ eV, Table IV.

In ethane, $\sigma(VCH^+)$ rises steeply. The mean threshold of this cross section is 3.47 ± 0.04 eV. This product can be formed as the result of a decomposition of VCH_2^+ (process 17) or VCH_3^+ (reaction 18). Because $\sigma(VCH_2^+)$ decreases near 3 eV, 0.5 eV

$$V^+ + C_2H_6 \rightarrow VCH_2^+ + CH_4 \rightarrow VCH^+ + H + CH_4 \quad (17)$$

$$\rightarrow VCH_3^+ + CH_3 \rightarrow VCH^+ + H_2 + CH_3 \quad (18)$$

below the threshold of $\sigma(VCH^+)$, and because at 3.5 eV $\sigma(VCH_3^+) \sim 10\sigma(VCH_2^+)$, it is probably more likely that the source of VCH^+ is reaction 18. Reaction 17 yields a bond energy of 4.98 ± 0.04 eV, while in process 18 a bond energy for $V^+–CH$ of 5.02 ± 0.04 eV is obtained. The ethane data thus indicate that $D°(V^+–CH) = 5.00 \pm 0.06$ eV, about 1.3 eV higher than the value obtained from the ethyne system. This higher value is reaffirmed in an unpublished study of the reaction of V^+ with methane,[34] where we find a bond energy of 4.86 ± 0.11 eV.

In the reaction of V^+ with ethene, VCH^+ can be formed in processes 19, 20, or 21. This system can provide additional evidence for the larger value of $D°(V^+–CH)$, even though the cross section for VCH^+ is difficult to fit due to its small size and the resultant noise in the base line. However, close inspection of

$$V^+ + C_2H_4 \rightarrow VCH^+ + CH_3 \quad (19)$$

$$\rightarrow VCH_3^+ + CH \rightarrow VCH^+ + H_2 + CH \quad (20)$$

$$\rightarrow VCH_2^+ + CH_2 \rightarrow VCH^+ + H + CH_2 \quad (21)$$

Figure 7 reveals an apparent threshold near 1.8 eV. This is a reasonable lower limit to the true threshold. Accounting for the threshold lowering effects of excited V^+ ions, 0.08 eV, and the Doppler broadening, 0.6 eV, we can estimate the upper limit to the threshold energy as 2.5 eV. If $D°(V^+–CH) = 5.00$ eV, the predicted threshold for reaction 19 is 2.07 eV. Other processes, reactions 20 and 21, have much higher thresholds, 6.80 eV each. If the lower value for the VCH^+ bond energy, 3.71 eV, is used, then the predicted thresholds for the above processes are 3.36 and 8.10 eV, respectively. Thus, the larger $V^+–CH$ bond energy is again implicated. Apparently, formation of VCH^+ in reaction 16 requires surmounting an activation barrier in excess of the endothermicity. This will be discussed further below.

In the ethane system, the vanadium carbyne ion has a second, high-energy feature which has an *apparent* threshold near 9 eV. The only reactions which have thresholds in this vicinity are eq 22, 23, and 24. These have ΔE's equal to 8.10, 8.23, and 8.37

$$V^+ + C_2H_6 \rightarrow VCH^+ + CH_3 + 2H \quad (22)$$

$$\rightarrow VCH^+ + CH + 2H_2 \quad (23)$$

$$\rightarrow VCH^+ + CH_2 + H_2 + H \quad (24)$$

eV, respectively. It is not possible to tell which of these reactions is the most likely from threshold analysis because of overlap from the cross section of reaction 18. However, process 22 is probably the most reasonable when the overall reaction mechanism is considered. This also will be discussed further below.

The final value adopted for $D°(V^+–CH)$ is the average of the ethane and methane result, 4.94 ± 0.09 eV. The accuracy of this value will be more easily judged when other metal ion–carbyne bond strengths are measured.

4. Vanadium Carbide Ion. Formation of VC^+ (Figure 8) occurs in all reaction systems by decomposition of higher weight primary ions. Both reactions 25 and 26 correspond to decomposition of the most abundant primary ion, VCH_2^+ and VCH^+, respectively.

$$V^+ + C_2H_4 \rightarrow VC^+ + CH_2 + H_2 \quad (25)$$

$$V^+ + C_2H_2 \rightarrow VC^+ + CH + H \quad (26)$$

In both systems, the data rise steeply. It is reproduced by both linear ($m = 0$, $n = 1$) and line-of-centers ($m = n = 1$) fits. Analysis of the thresholds for VC^+ formed in reactions 25 and 26 yields $D°(V^+–C) = 3.96 \pm 0.04$ eV and 3.97 ± 0.15 eV. These bond energies are in excellent agreement with the result of an unpublished study of reaction 27,[34] where a value of 3.94 ± 0.03 eV was obtained.

$$V^+ + CO \rightarrow VC^+ + O \quad (27)$$

In the ethane system, Figure 2, there are several pathways for producing VC^+: dehydrogenation of VCH_2^+ made in process 14 or 15 (reactions 28 and 29), and H-atom loss from VCH^+ formed

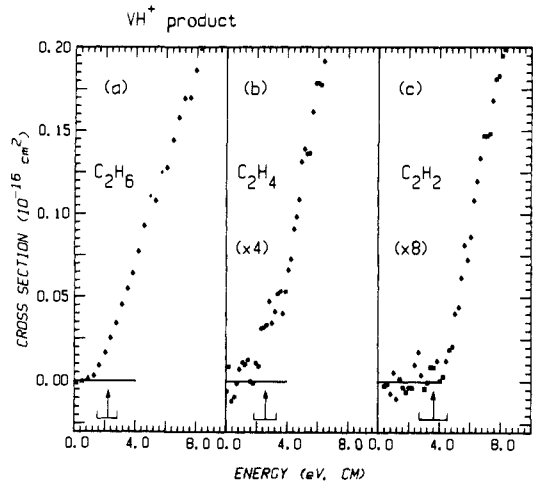

Figure 9. Threshold regions of $\sigma(VH^+)$ as observed in (a) $V^+ + C_2H_6$ (▲), (b) $V^+ + C_2H_4$ (●), and (c) $V^+ + C_2H_2$ (■). Arrows indicate the predicted thresholds. Note that the x-axis energy scale is discontinuous. The magnitude of the energy broadening at threshold is shown by the horizontal error bars.

in process 17 (reaction 30) or 18 (reaction 31). Note that reactions 29 and 31 are the same overall process. Because VC^+ is formed

$$V^+ + C_2H_6 \rightarrow VCH_2^+ + CH_4 \rightarrow VC^+ + H_2 + CH_4 \quad (28)$$

$$\rightarrow VCH_2^+ + CH_3 + H \rightarrow VC^+ + H_2 + CH_3 + H \quad (29)$$

$$V^+ + C_2H_6 \rightarrow VCH^+ + H + CH_4 \rightarrow VC^+ + 2H + CH_4 \quad (30)$$

$$\rightarrow VCH^+ + H_2 + CH_3 \rightarrow VC^+ + H + H_2 + CH_3 \quad (31)$$

as a decomposition product of a secondary process, $\sigma(VC^+)$ is small and scattered, making detailed analysis difficult. Use of the vanadium carbide ion bond strength derived above predicts that the endothermicity of reaction 28 is 3.57 eV. A line-of-centers fit using this threshold is consistent with the data of the low-energy feature in VC^+ in Figure 2. Reactions 29 (reaction 31) and 30 have expected thresholds at 8.09 and 8.05 eV. Since no other processes forming VC^+ have onsets in this vicinity, we attribute the high-energy peak of $\sigma(VC^+)$ to these reactions.

5. Vanadium Hydride Ion. Accurate determination of the thermochemistry of VH^+ is difficult because of experimental problems in resolving the hydride from the $\sim 10^5$ times more intense reactant signal near threshold. Consequently, quantitative endothermicities for processes producing this ion were not obtained. A previous study of $V^+ + H_2$, HD, and D_2[17] shows that the V^+–H bond energy is 2.09 ± 0.05 eV.[36] When this value is used, the predicted thresholds of H-atom abstraction from C_2H_6, C_2H_4, and C_2H_2 are 2.20, 2.61, 3.60 eV, respectively. As can be seen in Figure 9, the data are consistent with these predictions if energy-broadening effects are considered. In both the C_2H_4 and C_2H_2 systems, $\sigma(VH^+)$ has a second, higher energy feature (Figures 3a and 4) which seems to correspond to breaking of the C–C bond, reactions 32 and 33. Process 32 has a calculated onset at 9.9 eV and process 33 has one at 11.3 eV. These reactions could be

$$V^+ + C_2H_4 \rightarrow VH^+ + CH + CH_2 \quad (32)$$

$$V^+ + C_2H_2 \rightarrow VH^+ + C + CH \quad (33)$$

decompositions of the primary reaction products in these systems, VCH_2^+ and VCH^+, respectively.

6. $VC_2H_r^+$: Endothermic Products. Figure 10 shows the threshold regions of the endothermically produced $VC_2H_r^+$ ions. VC_2^+ and VC_2H^+ are formed in the reaction of V^+ with ethyne,

(36) The 298 K value of $D°(V^+–H)$ cited in Table II is $3kT/2 = 0.04$ eV higher than that given in ref 17, $D°_0(V^+–H) = 2.05$ eV.

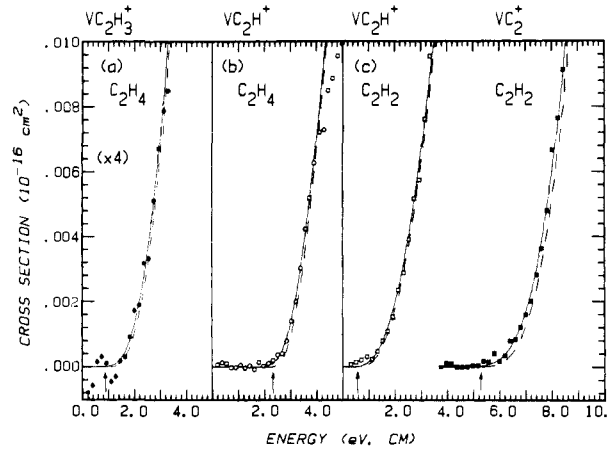

Figure 10. Threshold regions for endothermically produced $VC_2H_r^+$: (a) $VC_2H_3^+$ (●) and (b) VC_2H^+ (○) formed from $V^+ + C_2H_4$, (c) VC_2H^+ (□), and VC_2^+ (■) formed from $V^+ + C_2H_2$. The solid lines are calculated fits, convoluted over the energy broadening. The dashed lines are the same fits with no convolution. Arrows indicate the derived threshold energies.

while V^+ + ethene yields VC_2H^+ and $VC_2H_3^+$. The best fits for $\sigma(VC_2H^+)$ formed from ethyne in reaction 34, Figure 10c, yield

$$V^+ + C_2H_2 \rightarrow VC_2H^+ + H \quad (34)$$

a threshold of 0.55 ± 0.10 eV and thus a V^+–C_2H bond energy of 5.13 ± 0.10 eV. In the ethene system, Figure 10b, reaction 35 has a threshold of 2.31 ± 0.13 eV which yields a bond energy in excellent agreement, 5.18 ± 0.13 eV. A second, high-energy

$$V^+ + C_2H_4 \rightarrow VC_2H^+ + H_2 + H \quad (35)$$

feature in the ethene system is observed near 10 eV, Figure 3a. This can only correspond to reaction 36, which has a calculated threshold of 6.8 eV.

$$V^+ + C_2H_4 \rightarrow VC_2H^+ + 3H \quad (36)$$

The product VC_2^+, Figure 10c, can be formed by C_2H_2 dehydrogenation, process 37, or by elimination of two H atoms, reaction 38. The identity of the neutrals and $D°(V^+–C_2)$ can be determined by thermochemical arguments. The best fits have

$$V^+ + C_2H_2 \rightarrow VC_2^+ + H_2 \quad (37)$$

$$\rightarrow VC_2^+ + 2H \quad (38)$$

a mean threshold of 5.23 ± 0.15 eV. If VC_2^+ is formed by dehydrogenation, then $D°(V^+–C_2)$ equals 0.96 eV. This means that $D°(VC_2^+–H) = 9.23$ eV (213 kcal/mol). This is much larger than comparable C–H bond energies, $D°(H–C_2H) = 133$ kcal/mol or $D°(VC^+–H) = 106$ kcal/mol. Thus, the neutral products must be two hydrogen atoms, giving $D°(V^+–C_2) = 5.48 \pm 0.15$ eV (126 ± 4 kcal/mol) and $D°(VC_2^+–H) = 109$ kcal/mol, a much more reasonable value. Thus, VC_2^+ is formed exclusively by reaction 38.

$VC_2H_3^+$ formed from ethene in reaction 39, Figure 10a, has a mean threshold of 0.89 ± 0.20 eV. This yields $D°(V^+–C_2H_3) = 3.80 \pm 0.20$ eV. Because VC_2^+ and $VC_2H_3^+$ are each seen

$$V^+ + C_2H_4 \rightarrow VC_2H_3^+ + H \quad (39)$$

in only one reaction system, the possible presence of activation barriers cannot be checked. The bond energies in Table II for these two ions are most conservatively viewed as lower limits.

7. $VC_2H_r^+$: Exothermic Products. The only two exothermic processes observed in this study are dehydrogenation of ethane to make $VC_2H_4^+$, reaction 40, and of ethene, process 41, producing $VC_2H_2^+$. The former is shown in Figure 2 and in more detail in Figure 11. Process 41 is shown in Figure 3a and in detail in Figure 12.

$$V^+ + C_2H_6 \rightarrow VC_2H_4^+ + H_2 \quad (40)$$

$$V^+ + C_2H_4 \rightarrow VC_2H_2^+ + H_2 \quad (41)$$

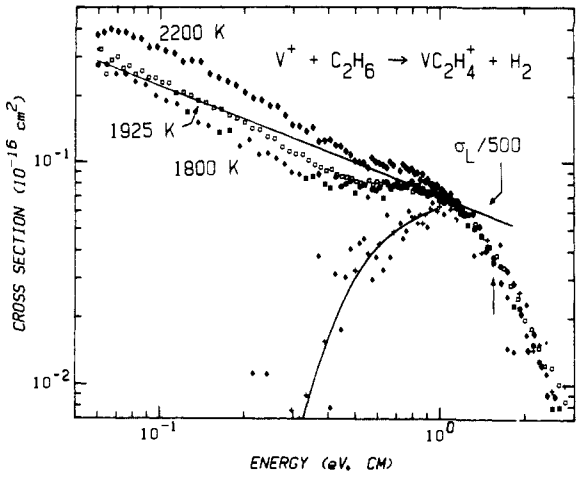

Figure 11. Cross sections of reaction 40 shown at three ion source filament temperatures, 1800 K (●), also shown in Figure 2, 1925 K (□), and 2200 K (♦). The symbols (+) represent $\sigma(VC_2H_4^+)$ with the exothermic part removed (see text). The line through these points is a polynomial fit. The arrow marks the onset of reaction 42. Also shown is $\sigma_L/500$, eq 5.

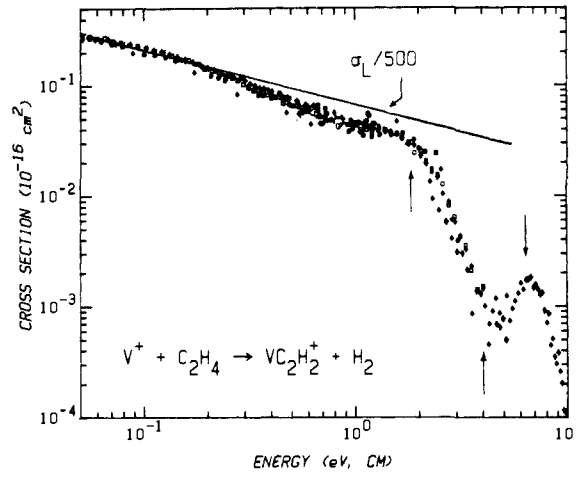

Figure 12. Energy dependence of the cross section for reaction 41 at three ion source filament temperatures: 1800 K (●), 1925 K (□), and 2200 K (♦). Arrows indicate the onsets of reactions 43, 44, and 45. The solid line is $\sigma_L/500$, eq 5.

In the ethane system, the low-energy cross section for reaction 40 is about 500 times smaller than predicted by the LGS formula, eq 5. To test whether this is the result of producing a high-energy isomer of the $VC_2H_4^+$ product, the reaction of V^+ with CH_3CD_3 was examined. The only product observed is due to loss of HD, $VCH_2CD_2^+$. This implies that the dehydrogenation forms a vanadium ion ethene complex rather than a vanadium ethylidene ion, the result of a 1–1 dehydrogenation.

Another possible explanation for the extremely small cross section is that this reaction is due exclusively to small amounts of excited states in the V^+ beam. Table I shows that the states above 1 eV are present in approximately the correct amount if they react at the collision limit. To test for this, experiments were conducted at several filament temperatures. Figure 11 shows that the magnitude of the cross section at low energies (<0.4 eV) is enhanced by a factor of about 1.6 in going from a filament temperature of 1800 to 2200 K. Below 0.2 eV, the energy dependence of the curves is $E^{-0.5}$, and between 0.2 and 0.4 eV, the cross sections are proportional to $E^{-0.70\pm0.04}$, deviating from the LGS form. Above 0.4 eV, the temperature effect gradually decreases until about 1 eV. Beyond this energy, no effect is observed and the cross section falls off rapidly. These results strongly suggest that the exothermic dehydrogenation of ethane is due to excited states of V^+ but that above 0.4 eV the low-lying ^5F and ^5D states contribute. These data are inadequate to determine with certainty whether both quintet states are active at the higher energies. The rapid falloff at energies greater than 1.0 eV could be due to competition from reaction 14, beginning at 0.79 eV, but is probably mainly due to process 42, requiring 1.42 eV.

$$V^+ + C_2H_6 \rightarrow V^+ + C_2H_4 + H_2 \quad (42)$$

The component of the cross section due to the quintet states can be ascertained qualitatively by removing the exothermic part of the cross section. This is achieved by extrapolating the data in Figure 11 to a zero excited-state population. The result, also shown in Figure 11, has an apparent threshold of 0.32 ± 0.07 eV. Correcting for the average electronic energy of the V^+ (0.07 eV, excluding higher states) and the Doppler broadening of 0.25 eV, the lower and upper limits of the threshold are 0.2 and 0.7 eV. This yields a vanadium ion–ethene bond energy between 0.7 and 1.2 eV (16–28 kcal/mol), assuming that there are no activation barriers and that the neutral product is molecular hydrogen. The alternate assumption that two hydrogen atoms are produced yields a value for $D°(V^+–C_2H_4)$ which is larger by 4.5 eV. This is an unusually high and unlikely value.

Previous measurements of transition-metal ion–ethene bond energies have been made for Sc^+, Ti^+, Fe^+, Co^+, and Ni^+. C_2D_4 has been found to displace CO from $FeCO^+$ and $NiCO^+$, yielding $D°(Fe^+–C_2D_4) > 1.63$ eV[6a] and $D°(Ni^+–C_2D_4) = 2.2 \pm 0.2$ eV.[6b] Scandium and titanium ions are observed to exothermically dehydrogenate ethane, making $D°(M^+–C_2H_4) \geq 1.42$ eV. Interpolation between nickel–ethene ion and lithium–ethene ion (0.78 ± 0.22 eV) bond strengths led to an estimate of 1.7 ± 0.2 eV for Sc^+–ethene.[8] The bond energy of Co^+ to C_2H_4 was estimated from two apparently conflicting results. $CoC_2H_4^+ + H_2$ formation from Co^+ + ethane has a threshold of less than 1 eV, suggesting that $D°(Co^+–C_2H_4) < 1.42$ eV.[1b] However, Co^+ + cyclopentane produced cobalt–ethene ion and propene exothermically, meaning that the $Co^+–C_2H_4$ bond energy is greater than 1.56 eV.[1c] Apparently, dehydrogenation of ethane by cobalt ions requires surmounting an activation barrier. It was estimated that this barrier is not large and, therefore, $D°(Co^+–C_2H_4)$ is given as 1.60 ± 0.10 eV.[1c] The value for Li^+ is a lower limit for metal ion–ethene bond energies, since this is a purely electrostatic interaction. In light of these numbers, a bond energy for $V^+–C_2H_4$ of 0.7–1.2 eV is anomalously low. This implies that the dehydrogenation of ethane by ground-state V^+, as with cobalt ions, has an activation barrier and that $D°(V^+–C_2H_4)$ probably exceeds 1.4 eV.

In the ethene system, the low-energy cross section is also about 500 times smaller than that predicted by the LGS formula, eq 5. The cross section falls off as $E^{-0.5}$ at low energies but deviates from LGS behavior above 0.2 eV, where it falls off as $E^{-0.72}$. One possibility is that the small cross section is also due to reactions of excited states of V^+. This was tested by examining the dependence of the cross section on the filament temperature. Since no effect is observed (Figure 12), we conclude that this reaction is primarily due to the low-lying ^5F and ^5D states and that reactions of both quintet and triplet states are inefficient.

At higher energies, $\sigma(VC_2H_2^+)$ falls off rapidly. The onset of this decrease corresponds nicely to the energy required for process 43, 1.81 eV. At still higher energies, the cross section rises,

$$V^+ + C_2H_4 \rightarrow V^+ + C_2H_2 + H_2 \quad (43)$$

indicative of a new endothermic channel. This must correspond to reaction 44. The fact that this feature begins to decrease at the thermodynamic limit for process 45, 6.3 eV, helps to verify this. Analysis of the threshold of this high energy feature is

$$V^+ + C_2H_4 \rightarrow VC_2H_2^+ + 2H \quad (44)$$

complicated by the presence of the exothermic channel. The best fits to the data give the threshold as between 3.9 and 4.2 eV. This

$$V^+ + C_2H_4 \rightarrow V^+ + C_2H_2 + 2H \quad (45)$$

gives $D°(V^+–C_2H_2) = 2.20 \pm 0.21$ eV. This is consistent with the lower limit of 1.81 eV established by observation of the exothermic channel. This value also seems reasonable in light

of the metal ion–ethene bond energies discussed above.

For comparison with experiments conducted only at thermal energies, it is of interest to calculate the rate constant, k, for reactions 40 and 41. This is accomplished by using the expression $k = \langle \sigma v \rangle$, where v is the relative velocity of the reactants, σ is taken from the lowest filament temperature measurements, and the brackets indicate a convolution over a Maxwell–Boltzmann distribution of velocities. The rate constants at 300 K are calculated to be $1.9 \pm 0.4 \times 10^{-12}$ cm^3 s^{-1} for both reactions.

Ion Structure. The structures of VCH_r^+ ions can be confirmed by two independent arguments. First, as noted for other metal systems,[1b] the VCH_{r-1}^+–H bond energies, Table II, are much stronger than $D°(V^+–H) = 48$ kcal/mol. They are more comparable to carbon–hydrogen bonds that are "resonantly stabilized", e.g., $D°$(allyl–H) = 86 kcal/mol or $D°$(benzyl–H) = 88 kcal/mol.[37] For VCH_2^+–H, the stabilization is afforded by formation of the V–C π bond. A similar argument holds for VCH^+–H. In the case of VC^+–H, the bond energy of 106 kcal/mol is clearly too large for a metal hydride bond. Second, the primary decomposition route of all VCH_r^+ ions is dissociation to $V^+ + CH_r$, where the CH_r ligand is left intact. While secondary decomposition channels, such as loss of H or H_2 occur, they are minor pathways. This is demonstrated by the fact that $\sigma(VCH_r^+)$ decreases more rapidly than $\sigma(VCH_{r-1}^+)$ and $\sigma(VCH_{r-2}^+)$ increase, Figures 2, 3, and 4. We conclude that the VCH_r^+ ions are well-represented by structures in which no formal metal–hydrogen bonds exist. However, the possibility of "agostic" M–C–H interactions cannot be dismissed.

An analysis of the V^+–R bond dissociation energies in Table II reveals that they increase as their expected bond order increases. Thus, $D°(V^+–CH_3) \sim D°(V^+–H) < D°(V^+–CH_2) < D°(V^+–C) < D°(V^+–CH)$. The amount of increase is proportional to that observed in organic chemistry and is roughly quantified by eq 46.

$$D°(V^+–R) \sim 0.5[D°(R–R)] \quad (46)$$

Similar proportionalities for ScR^+, TiR^+, and CrR^+ have been compiled in our laboratory.[34] This provides us with a very useful device for quantifying bond order and demonstrates that the bond energies truly represent singly bonded V^+–H and V^+–CH_3, doubly bonded V^+=C and V^+=CH_2, and triply bound V^+≡CH.

Unlike VCH_r^+ species, V^+–C_2H_r bonds do not decrease with increasing r. A somewhat erratic pattern exists. Based on comparisons with V^+–CH_r bond energies, V^+–C_2H_2 is as strong as a single bond, V^+–C_2H_3 is as strong as a double bond, and V^+–C_2H and V^+–C_2 are as strong as triple bonds. This assumes that a C–C interaction is maintained in all cases. Analysis of the C–C bond strengths in $VC_2H_r^+$ indicates that this is true. For example, in VC_2^+, the VC^+–C bond energy is 180 kcal/mol, nearly twice $D°(V^+–C) = 91$ kcal/mol. This rules out a dicarbide structure.

Based on the strength of the metal–ligand bond, $VC_2H_3^+$ cannot be a simple vanadium vinyl ion. Overlap between the C–C π bond and V^+ orbitals must be occurring. This is confirmed by the observation that the VCH^+–CH_2 bond has a bond order of only 1.5. One attractive possibility for the structure of this ion is the allylic-like species, **1**. Similar considerations should apply to the

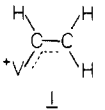

1

VC_2H^+ ion. The triple bond character of the V–C bond rules out a simple vanadium–ethylidyne ion. Delocalization of the C–C π bonds is also indicated by the VC^+–CH bond order of 2.5. Structure **2** shows one possibility which could explain such observations.

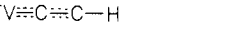

2

In contrast to these strongly bound radical ligands is the stable ethyne. V^+–C_2H_2 has only the strength of a single bond. This

Scheme I

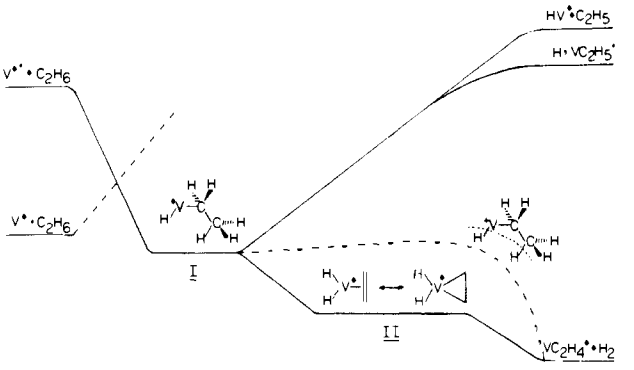

is consistent with a simple dative interaction, **3**, but can also be explained by the metallocyclopropene, **4**. The same overall

3 **4**

thermochemistry is maintained since in the latter structure, two V–C single bonds (50 kcal/mol each) are formed and one C–C π bond ($\sim$56 kcal/mol) is broken. The VCH^+–CH bond order of 2 can also be explained by either **3** or **4**. The electronic character of these species should also be noted. While **3** maintains the spin multiplicity of the V^+ ion (that is, it can be in a quintet, triplet, or singlet state), **4** uses two V^+ electrons in bonding and therefore can only be in a triplet or singlet state.

The remaining $VC_2H_r^+$ species seen in these studies, $VC_2H_4^+$, unfortunately has no definitive thermochemical information to aid its structural characterization. As noted above, the bond energies of other metal ion–C_2H_4 species are comparable to our measured value for V^+–C_2H_2. Thus, we expect a similar value for $D°(V^+–C_2H_4)$ and in Table II assign an estimate of 50 kcal/mol. Analogous structures, **5** and **6**, are also proposed. Again, note that **5** can be in a quintet, triplet, or singlet state, but **6** cannot be in a quintet state.

5 **6**

Reaction Mechanisms. In the following discussion, energy level schemes for reactions observed with $V^+ + C_2H_6$ and C_2H_4 are presented. Reaction intermediates are proposed based on thermochemical arguments and experimental results. Aside from these considerations, choices for reaction intermediates and products are limited by the fact that the vanadium ion can support four covalent bonds at most or equivalently that the highest oxidation state of V is +5. Since no direct experimental information is available for V^+ bound to more than one ligand, the bond energies for such species are assumed to be the same as for singly ligated V^+ species, Table II. A bond additivity assumption is not always appropriate but for the case of vanadium is probably sufficiently accurate to identify the general reactivity trends.

1. V^+ + Ethane. Schemes I and II show reaction coordinate diagrams similar to those proposed previously for the reaction of $Co^+ + C_2H_6$.[1b] The initial reaction step in Scheme I is C–H insertion and in Scheme II is C–C insertion. The possibility of its application when Co^+ is replaced by V^+ is addressed here. Insertion of V^+ into a C–H bond forms intermediate I. The ΔH of this step is calculated to be -3 ± 3 kcal/mol, based on a preliminary value for $D°(V^+–C_2H_5) = 56 \pm 3$ kcal/mol from a study of V^+ + propane.[34] From I, the lowest energy products, $VC_2H_4^+ + H_2$, can be produced either by a concerted five-center H_2-elimination or via formation of intermediate II followed by reductive elimination of H_2. Since I must be in a triplet state, an intersystem crossing is necessary to form this intermediate from ground-state V^+. This may explain the barrier to $VC_2H_4^+$ formation from V^+ (^{5}D and ^{5}F) as well as the efficiency with which the triplet states of V^+ undergo this reaction.

Scheme II

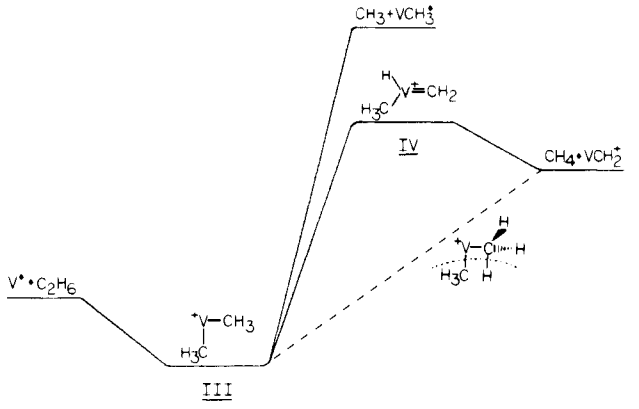

At higher energies, I can decompose directly to VH^+, reaction 47, or to $VC_2H_5^+$, reaction 48. Direct experimental evidence of

$$V^+ + C_2H_6 \rightarrow VH^+ + C_2H_5 \quad (47)$$

$$\rightarrow VC_2H_5^+ + H \quad (48)$$

intermediate I being a common precursor to both $VC_2H_4^+$ and VH^+ would occur if $\sigma(VC_2H_4^+)$ decayed near the threshold of $\sigma(VH^+)$. Unfortunately, as noted above, the cross section for $VC_2H_4^+$ falls sharply at approximately 1.0 eV, 1.2 eV less than ΔE of $VH^+ + C_2H_5$ production.

Reactions 47 and 48 are nearly isoergic, yet the latter is not observed. This is also true for all other first-row metals except Cr^+ [34] where we have observed that $\sigma(CrC_2H_5^+)$ is about 25 times smaller than $\sigma(CrH^+)$. There are several possible reasons for this. The first is that metal hydride ion could be formed by direct abstraction. Thus, the precursor to $MC_2H_5^+$, intermediate I, may not exist at the energies required to form MH^+ or $MC_2H_5^+$. Alternatively, the frequency factor for $MC_2H_5^+$ may be much smaller than that for MH^+. While this is probably true, it seems unlikely that it is an order of magnitude smaller, as required to explain the data. The most probable explanation involves angular momentum constraints. The orbital angular momentum of the reactants is given by $L = \mu v b$, where μ is the reduced mass, v is their relative velocity, and b is the impact parameter. The rotational angular momentum, J, is small compared to L and is neglected. Similar quantities for products are denoted by primes. Angular momentum conservation requires that $L' + J' = L$. For the endothermic reactions considered here, $E' < E = \mu v^2/2$. In reaction 47, $\mu' \sim \mu$, therefore, in the limit that $J' = 0$, $b' = \mu v b/\mu' v' > b$. For reaction 48, $\mu' \sim \mu/19$, and $b' > 19^{1/2} b$. Since the product impact parameters are restricted to molecular dimensions, b must be very small in order for the magnitude of b' to be physically realistic. Thus, the cross section, $\sigma = \pi b^2$, of forming $VC_2H_5^+ + H$ is predicted to be smaller than $\sigma(VH^+)$ by a maximum factor of about 19. Rotational effects can mediate this large factor, but our general expectation remains that $\sigma(VC_2H_5^+)$ will be small.

The second lowest energy channel is production of $VCH_2^+ + CH_4$, reaction 14. Methane elimination has been noted only once previously (although not quantified) in reactions of Co^+ and C_2H_6;[1b] however, this behavior has also been observed in our preliminary studies of the reactions of Sc^+, Ti^+, and Cr^+ with C_2H_6. Methane elimination can occur in three ways. An α-methyl shift in I or an α-hydrogen shift in III can both produce intermediate IV, which can then reductively eliminate CH_4. Alternatively, a four-center elimination from III could be involved. Because $\sigma(VCH_2^+)$ changes slope near the threshold of $VCH_3^+ + CH_3$ formation, well before any decomposition channels open, both VCH_2^+ and VCH_3^+ must have a common intermediate precursor, presumably III. There are several reasons why IV is an unlikely intermediate in this reaction. First, Scheme II shows that our calculations predict an activation barrier in excess of the endothermicity of reaction 14 to form IV. Since the observed threshold yields a V^+–CH_2 bond energy consistent with that obtained in reaction 13 in the ethene system, no such barrier is apparent. Second, conversion of III to IV formally requires an intersystem crossing from a triplet to a singlet surface. Further, production of $VCH_2^+ + CH_4$ requires crossing back to a triplet surface. Third, we have observed demethanation of C_2H_6 by Sc^+ and Ti^+.[34] Since neither of these can support the four bonds in IV, this intermediate is unlikely in these systems. If V^+ reacts in a fashion analogous to Sc^+ and Ti^+, then a four-center elimination step from III is the more likely reaction mechanism. This reaction step, a symmetry-forbidden process in organic chemistry, is viable in transition-metal chemistry owing to the d character in the metal–ligand bonds.[38]

Symmetric C–C bond cleavage, process 10, is the major reaction between ethane and all metal ions that have been studied thus far.[1,8,9] This is presumed to proceed via formation of intermediate III which is exothermic by 10 ± 3 kcal/mol. As suggested above for C–H insertion, a barrier to formation of III due to an intersystem crossing could also exist here. However, all reaction channels available to III probably have endothermicities in excess of this barrier. Thus, no direct experimental evidence of it would be seen. In the Sc^+ and Ti^+ systems, barriers to demethanation are observed and may be evidence for such an intersystem crossing in C–C insertion processes.[39]

Decomposition of VCH_2^+ and VCH_3^+ give rise to all other products observed in this system. The lowest energy decomposition of VCH_2^+ is dehydrogenation, shown by the low-energy feature in $\sigma(VC^+)$ in Figure 2. Alternate decomposition pathways are sequential loss of hydrogen atoms, shown by the low-energy peak in $\sigma(VCH^+)$ and the second high-energy feature of $\sigma(VC^+)$. It is interesting to note that in both $\sigma(VCH^+)$ and $\sigma(VC^+)$, the low-energy peak occurs between 4 and 5 eV. This can be attributed to loss of the VCH_2^+ precursor in both cases, since metal–ligand cleavage in VCH^+ and VC^+ can't begin until 8.2 and 7.6 eV, respectively. As noted above, this indicates that V^+–CH_2 bond dissociation is the most favorable decay route once it is energetically allowed.

The lowest energy decomposition pathway available to VCH_3^+ is loss of H_2 at 3.54 eV. This reaction is inefficient, since $\sigma(VCH_3^+) \sim 20\sigma(VCH^+)$ but probably accounts for most of the formation of VCH^+ at low energies. H loss from VCH_2^+, mentioned above, may be a minor pathway. It is evident that vanadium methyl ion decomposes primarily by cleavage of the metal–ligand bond, beginning at $\Delta E' = 3.92$ eV. It should be noted that this process begins as soon as it is thermodynamically allowed. A secondary decomposition pathway is hydrogen atom loss to form VCH_2^+. This also begins near its thermodynamic limit, 5.4 eV. These observations show that there is a finite probability that all excess energy in $VCH_3^+ + CH_3$ formation is in internal modes of the ionic product. This indicates that the process is not merely a spectator stripping type of reaction but rather involves a broad distribution of energy among translational and internal modes. This appears inconsistent with the direct process model used to fit this cross section. This suggests that the use of such a model need not imply anything concerning reaction dynamics.

High-energy production of MCH_2^+ has been observed previously with Ni^+.[1d] This study is the first where both paths of metal carbene ion formation, demethanation of ethane, reaction 14, and decay of MCH_3^+, reaction 15, are observed. The VCH_2^+ formed at high energy can also decompose further by H and H_2 loss to produce the high-energy features of VCH^+, reaction 22, and VC^+, reaction 29. The alternate pathways to form VCH^+, reactions 23 and 24, are unlikely since no viable precursor corresponding to these processes is observed. VC^+ can also be formed at high energies by reactions 30 and 31. These ions in turn decay to

(37) McMillen, D. F.; Golden, D. M. *Annu. Rev. Phys. Chem.* **1982**, *33*, 493–532.

(38) Upton, T. H.; Rappe, A. K. *J. Am. Chem. Soc.* **1985**, *107*, 1206–1218.

(39) In examining Scheme II, it also seems possible that these barriers might be related to the formation of IV. However, as noted above, neither Sc^+ nor Ti^+ can produce IV with four covalent bonds. Formation of IV is therefore much more energetically unfavorable for these systems than is shown for V^+. Such large barriers are inconsistent with the experimental results.

Scheme III

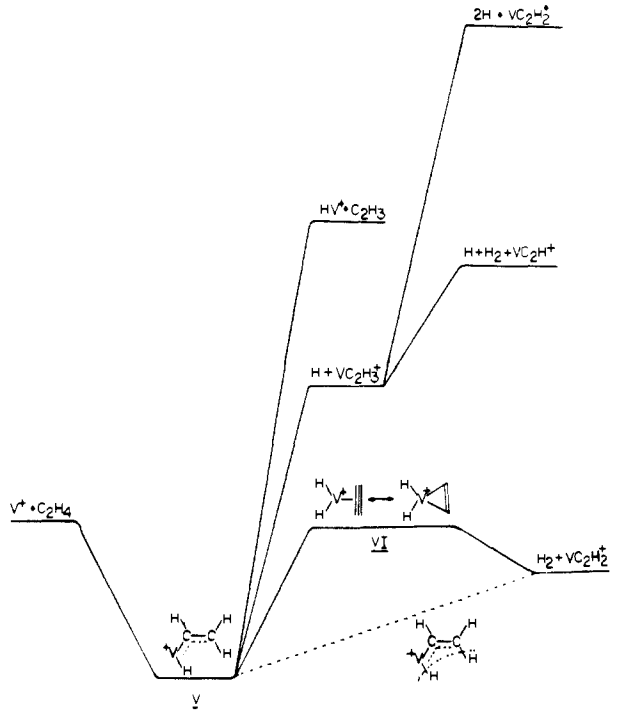

Scheme IV

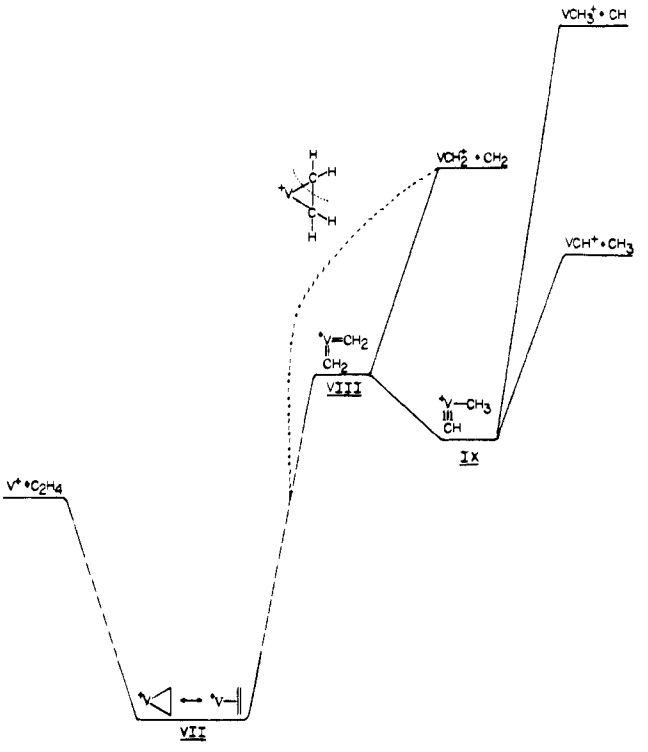

re-form V^+ at ~13 and ~12 eV, respectively.

2. V^+ + Ethene. Schemes III and IV present reaction coordinate diagrams for the V^+ + ethene system. The most detailed literature study of an atomic metal ion–ethene reaction, with Co^+, showed only two reaction channels, production of $CoH^+ + C_2H_3$ and $CoCH_2^+ + CH_2$.[1a] While these channels are likewise the most likely endothermic processes for V^+, a number of additional reactions are observed.

The lowest energy reaction path in V^+ + ethene is dehydrogenation, reaction 41. Unlike dehydrogenation of ethane by ground-state V^+, this reaction proceeds without a barrier. This may be because intermediate V, which is much more strongly bound than I, may provide a mechanism for intersystem crossings. Such crossings may be fairly inefficient, however, since, as noted above, reaction 41 occurs only once every 500 collisions. A more likely reason for the inefficiency may be that formation of **5**, the π complex, is the thermodynamically favored first step. Once **5** is formed, access to the C–H bonds is hindered. Alternatively, the inefficiency could be due to steric constraints, either in a five-center elimination step from intermediate V or in the β-H-transfer step for forming VI from V. Calculations show that formation of VI from $V^+ + C_2H_4$ is ~1 ± 5 kcal/mol exothermic.

Intermediate V is a reasonable precursor for several other products: $VC_2H_3^+$ (reaction 39), VH^+, $VC_2H_2^+$ (reaction 44), and VC_2H^+ (reaction 35). The first two are produced by cleavage at the V^+–H or V^+–C bond. The second two are secondary products formed by loss of H or H_2 from $VC_2H_3^+$. There is much evidence showing that these species share a common intermediate. The peak of $\sigma(VC_2H_3^+)$ occurs at $\Delta E' = 3.3$ eV, indicating that this product decreases either from competition by VH^+ formation at 2.65 eV or by dehydrogenation to VC_2H^+, at 2.31 eV. Decomposition of $VC_2H_3^+$ to $VC_2H_2^+ + H$ cannot occur until 4.05 eV or to $V^+ + C_2H_3$ until 4.77 eV.

As in the case of competition between VH^+ and $VC_2H_5^+$ in the V^+ + ethane system, VH^+ formation is favored over $VC_2H_3^+$ by angular momentum conservation requirements. This may be one reason that the peak magnitude of VH^+ is ~20 times larger than that of the peak of $VC_2H_3^+$, Figure 3a. That $VC_2H_3^+$ is seen at all is presumably due to the fact that it's energetically favored over VH^+ by 1.76 eV.

VC_2H^+ can be formed at low energies by H loss from $VC_2H_2^+$ formed in reaction 41 and H_2 loss from $VC_2H_3^+$ as noted above. It is not obvious whether both processes are occurring, but it is interesting that the VC_2H^+ cross section is larger than that of either potential precursor. Thus, it seems that $VC_2H_3^+$ and $VC_2H_2^+$ decay primarily by C–H, rather than V^+–CC or VC^+–C bond cleavage. This may be due to the strength of the interaction of V^+ with the C–C π cloud.

At about 7 eV, both $\sigma(VC_2H_2^+)$ and $\sigma(VC_2H^+)$ decrease. The former product can dissociate to $V^+ + C_2H_2$ at 6.3 eV, but H loss, commencing at 6.8 eV, must contribute to its decrease, as evidenced by the high-energy peak of VC_2H^+, reaction 36. VC_2H^+ probably decomposes by V^+–C_2H bond breakage which has a threshold at 7.6 eV (if the neutral products are H_2 + H) and 12.1 eV (if three H are formed). These correspond nicely to the low- and high-energy peaks in $\sigma(VC_2H^+)$.

The symmetric C–C bond cleavage product, VCH_2^+, can be formed directly from VII or via intermediate VIII, the dicarbene. If VIII exists, then by analogy to VO_2^+ it is most likely a bent molecule,[35] since this allows a double bond to each CH_2. The shape of the VCH_2^+ cross section at threshold has a very slow rise. This suggests that the available energy is distributed among many rovibrational modes and efficient C–C cleavage is hindered. In examining Scheme IV, we see that there are potential wells on either side of VIII, containing VII and IX. It is possible that the presence of these wells has a strong effect on the rate of VCH_2^+ production. Decomposition of VCH_2^+ by cleavage of the metal–carbon bond can begin at 7.56 eV, but the peak in the cross section comes closer to 9 eV. This means that either more energy is carried away in translation or that the CH_2 neutral product absorbs much internal energy, consistent with the slow rise in the threshold region. Decay channels other than loss of CH_2, such as loss of H or H_2 to make VCH^+ or VC^+, are not obvious but cannot be excluded. Loss of CH, reaction 32, could explain the secondary rise in $\sigma(VH^+)$ beginning near 10 eV.

Hydrogen atom transfer from the dicarbene to make intermediate IX gives access to the rearrangement channels producing both $VCH^+ + CH_3$, reaction 19, and $VCH_3^+ + CH$, reaction 12. It is unlikely that the transition state in this step is a species similar to IV of Scheme I, i.e., **7**, as this puts the vanadium into a +7 oxidation state. However, since VIII is bent, a metal–hydride interaction may not be necessary. In order to provide good orbital overlaps to bond V^+ to both CH and CH_3, intermediate IX must also be bent. Cleavage of one of the metal–ligand bonds leads to the observed rearrangement products. Given the difference

7

in bond energies between V^+–CH and V^+–CH_3 (64 kcal/mol), it is amazing that the latter ion is formed at all. This could mean that 1–3 hydrogen shifts along the C–V^+–C backbone are rather facile. Then, the metal carbyne, carbene, and methyl are all formed in competitive processes.

VCH^+ and VCH_3^+ have a number of possible decay routes. Vanadium carbyne ion can decay by losing H or CH, requiring at least 6.8 or 7.15 eV, respectively. High-energy routes to formation of VCH^+, primarily H loss from VCH_2^+ at 7.04 eV, also begin in this energy region. Vanadium methyl ion can lose molecular or atomic hydrogen, $\Delta E' \geq 6.80$ or 8.64 eV, or the methyl group, beginning at 7.14 eV.

The likely sources of VC^+ are the nearly isoenergetic dehydrogenation of VCH_2^+ and loss of H from VCH^+. The ratios of $\sigma(VC^+)$ to $\sigma(VCH_2^+)$ and $\sigma(VCH^+)$ are simiilar to those observed in the ethane system.

3. V^+ + Ethyne. In this system, the lowest energy process is C–H cleavage, producing $VC_2H^+ + H$. Elimination of H_2 is 3 ± 6 kcal/mol *more* endothermic than loss of H. Thus, the absence of dehydrogenation in this system is probably due to the decay of a necessary precursor, such as H–V^+–C_2H, before H_2 loss can occur. VC_2H^+ peaks at about 5.2 eV which must correspond to competition from the next lowest energy channels, formation of VH^+, at 3.6 eV, and VC_2^+, at 5.2 eV, since decomposition of VC_2H^+ to re-form the reactant V^+ requires at least 5.76 eV. $\sigma(VC_2^+)$ is clearly too small to account for all the decrease in $\sigma(VC_2H^+)$. This suggests that competition of VC_2H^+ and VH^+ formation is proceeding via intermediate **8**. This is confirmed

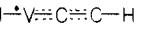

8

by noting that the decrease in $\sigma(VC_2H^+)$ is closely compensated by the increase in $\sigma(VH^+)$. The preference for formation of VH^+, once energetically accessible, is another indication of the angular momentum constraints discussed above for the hydrogen abstraction channels in the ethane and ethene systems.

At somewhat higher energies, VC_2H^+ decomposes to VC_2^+, reaction 38. The cross section for this ion, in turn, decreases near 10 eV. Only two dissociation channels are available. Dissociation to $V^+ + C_2$, requiring 10.8 eV, is the most reasonable since decay to $VC^+ + C$ cannot occur until 13.2 eV.

Symmetric C–C cleavage, reaction 16, is, as in the previous systems, the major process. Full insertion of V^+ in the C–C triple bond to form a dicarbyne species is unlikely, since this puts vanadium into a +7 oxidation state. The inability to cleave the C–C bond completely in a stable intermediate may explain the 1.3-eV barrier for reaction 16. Another consideration is the electronic character of the reaction. Since the ground-state V^+ is in a quintet state and ethyne in a singlet state, the reaction begins on a quintet surface. Ground-state products, however, are both doublets $[VCH^+(^2\Delta) + CH(^2\Pi)]$[40] which can arise only from a triplet or singlet surface. Thus, a surface crossing is required to form the products in their ground electronic states. Alternatively, excited states of either VCH^+ or CH could be involved. In particular, formation of CH ($^4\Sigma^-$), 0.74 eV[41] above ground state CH, would make the overall reaction spin-allowed.

VCH^+ decays primarily by breaking the vanadium–carbyne bond, starting at 10.9 eV. Secondary decomposition routes are loss of H to form VC^+ at 9.46 eV, reaction 26, or loss of C, producing VH^+ at 11.3 eV in process 33.

The threshold of vanadium carbide ion production requires the neutral products to be CH and H. These can be reached by decomposition of $VCH^+ + CH$ or $VC_2H^+ + H$. Since the latter products can decompose to $VC_2^+ + 2H$ and $V^+ + C_2H + H$ at energies far below that required for VC^+ formation, it is most likely that vanadium carbide originates exclusively from VCH^+ decay.

4. C–C vs. C–H Activation. A question of substantial interest in the systems studied here is whether C–H and C–C bond activation processes compete; that is, do they share a common intermediate. In ethane, C–H cleavage processes are most easily explained by using oxidative addition of a C–H bond to V^+ (i.e., production of I) followed by subsequent reactions. That such a process can and does occur seems to be unquestioned. Likewise, C–C cleavage processes, including the competition between VCH_2^+ and VCH_3^+ formation, are cleanly described by using intermediate III. Oxidative addition of the C–C bond, however, is not as readily accepted as that of the C–H bond. It is possible that III is not formed directly, but only by conversion of I to III via IV. However, if such a conversion were occurring, it is hard to understand why formation of VCH_3^+ would dominate VCH_2^+ since the former process would then require more extensive rearrangement. In addition, we find no direct indications of competition between C–H and C–C cleavage processes in the cross sections measured. Further, oxidative addition of the C–C bond to V^+ is thermodynamically favored by 7 ± 4 kcal/mol over C–H addition. This offers a straightforward rationale for the dominance of C–C cleavage processes in ethane. Taken together, these observations argue for believing that C–H *and* C–C oxidative addition to V^+ are both primary reaction steps. Subsequent transformations would proceed on separate potential energy surfaces, for example, those shown in Schemes I and II.

In both the ethene and ethyne systems, the dominance of C–C cleavage over C–H cleavage can be attributed to the strong bonding interaction between V^+ and the C–C π cloud. Once **5** (VII) and **3**, the thermodynamically favored intermediates, are formed, reaction is directed toward the C–C bond and access to the C–H bonds is hindered. Since the onsets of the major products, VCH_2^+ and VCH^+, show no influence on the cross sections of other products, no coupling of C–H and C–C chemistry is indicated. This implies that C–H cleavage chemistry proceeds via separate intermediates, V in the ethene system and **8** in ethyne.

Summary

The general results of this work indicate that vanadium ions cleave both carbon–carbon and carbon–hydrogen bonds. In all the C_2H_{2p} (p = 1–3) systems studied here, the major products are $VCH_p^+ + CH_p$, formed from symmetric cleavage of the C–C bond. For ethane and ethene, these endothermic reactions begin at the thermodynamic limits. For ethyne, an activation barrier is observed and attributed to electronic considerations. The second major process is formation of $VH^+ + C_2H_{2p-1}$. No evidence is found for competition between C–C and C–H cleavage reactions. The only exothermic channels observed, dehydrogenation of ethane and ethene, are inefficient. In the former system, this is due to an activation barrier for reactions of ground-state V^+. There is indication that these results may be due to a need for intersystem crossings.

The thermochemistry is used to determine ion structures. In particular, a correlation between bond energy and bond order is found. Thus, VH^+ and VCH_3^+ have single bonds, VCH_2^+ and VC^+ have double bonds, and VCH^+ has a triple bond. In ions containing two carbon atoms, the carbon–carbon bonds are left intact. The strength of the vanadium ion–C_2H_r interactions suggests that substantial overlap between the C_2 π cloud and V^+ is occurring. All product ions (save VH^+) are shown to have no formal metal–hydrogen bonds.

This paper presents the most complete study of the gas-phase reactions of an atomic metal ion with a particular hydrocarbon to date. The study is unique because both major and minor product channels have been carefully quantified. This has allowed the thermochemistry (Table II) for various organometallic ions to be measured from several separate experiments. This increases

(40) The assignment of the VCH^+ state as the $^2\Delta$ is based on the observation that the $D°(V^+–CH)$ can be represented as a triple bond. This leaves one unpaired electron on the vanadium which is presumably in a 3dδ nonbonding orbital.

(41) Kasdan, A.; Herbst, E.; Lineberger, W. C. *Chem. Phys. Lett.* **1975**, *31*, 78.

(42) Moore, C. E. *Natl. Stand. Ref. Data Ser., Natl. Bur. Stand.* **1970**, *No. 34*, 1.

the accuracy of such measurements and enables activation barriers to be identified. In addition, a correlation of the appearance and disappearance of different products permits gross features of the potential energy surfaces to be ascertained.

Acknowledgment. This work is supported by the National Science Foundation under Grant No. CHE-8306511. Acknowledgement is also made to the Chevron Research Co. and Monsanto Co. for partial support.

Registry No. V^{3+}, 22541-77-1; ethane, 74-84-0; ethene, 74-85-1; ethyne, 74-86-2.

Fast Time-Resolved IR Spectroscopy: The Photolysis of *trans*-[η-$C_5Me_5Fe(CO)_2]_2$, the Detection of *cis*-[η-$C_5Me_5Fe(CO)_2]_2$, and the Activation Energy for Cis to Trans Isomerization

Barry D. Moore,† Martyn Poliakoff,* and James J. Turner*

Contribution from the Department of Chemistry, University of Nottingham, Nottingham NG7 2RD, England. *Received September 16, 1985*

Abstract: Fast (μs) time-resolved IR spectroscopy is used to follow the UV flash photolysis of *trans*-[Cp*Fe(CO)$_2$]$_2$ (Cp* = ηC_5Me_5) in cyclohexane solution at room temperature. The primary photoproducts observed on this time scale are Cp*Fe(CO)$_2$· (major product) and Cp*Fe(μ-CO)$_3$FeCp* (minor product). The Cp*Fe(CO)$_2$· radicals dimerize to reform both the cis and trans isomers of [Cp*Fe(CO)$_2$]$_2$. The previously unknown cis isomer, **2a**, decays into the thermodynamically more stable trans isomer, **1a**, by a first-order process with activation energy 68 ± 5 kJ mol^{-1}.

Although the first organometallic applications of time-resolved IR spectroscopy have only recently been reported, the technique has already led to significant results.[1] The experiments are similar to conventional microsecond UV flash photolysis but the reactive intermediates are detected by IR rather than UV–vis spectroscopy. This has a number of distinct advantages for organometallic systems. (1) The UV–vis absorption bands of organometallic intermediates are generally broad and structurally uninformative, while IR spectra, particularly ν(CO) bands of metal carbonyls, contain considerable structural information. (2) IR bands, even in the gas phase, are relatively narrow so that it is often possible to distinguish several different intermediates by scanning quite a restricted wavenumber region of the spectrum. (3) Matrix isolation experiments[2] have provided a large body of highly diagnostic IR data for organometallic intermediates and these data can often be used directly to identify transient species in time-resolved IR experiments.

Time-resolved IR is particularly fruitful in the elucidation of the photochemistry of dinuclear transition-metal carbonyls. While matrix isolation only supplies structural information about CO-loss products (radicals are not observed because the "cage effect" promotes recombination), time-resolved IR allows study of all the primary photoproducts. One can obtain a valuable insight into the relative importance of CO loss and metal–metal bond homolysis in each system,[3,6] and furthermore, the well-separated ν(CO) IR bands can be used to monitor the thermal reactions of the various photoproducts. We are currently exploring the reactivity of 17e$^-$ species, such as (ηC_5H_5)Fe(CO)$_2$·, toward various ligands.[6]

In this paper, we concentrate on a different aspect of dinuclear carbonyls, intramolecular isomerization. In particular, we contrast the behavior of [Cp*Fe(CO)$_2$]$_2$, Cp* = ηC_5Me_5, and its hydrogen analogue [(η-C_5H_5)Fe(CO)$_2$]$_2$. In room temperature solution only the trans isomer of [Cp*Fe(CO)$_2$]$_2$ (**1a**) is stable,[7] while [(η-C_5H_5)Fe(CO)$_2$]$_2$ exists as a mixture of both cis and trans isomers,[8] **2b** and **1b**. The interconversion of these two isomers, **2b** ⇌ **1b**, has been extensively studied by ^{1}H and ^{13}C NMR[8,9] and is one of the classic examples of fluxional behavior.

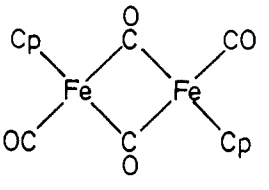

trans

1

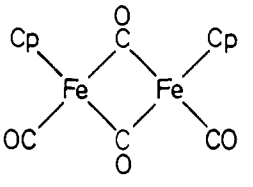

cis

2

a Cp = ηC_5Me_5

b Cp = ηC_5H_5

Here, we use time-resolved IR spectroscopy to show that the predominant photolytic process for *trans*-[Cp*Fe(CO)$_2$]$_2$ (**1a**) is formation of radicals Cp*Fe(CO)$_2$· and that both the cis and trans isomers **2a** and **1a** are formed when these radicals recombine. The

† Present address: Institute Le Bel, Université Louis Pasteur, 4 rue Blaise Pascal, 67000 Strasbourg, France.

(1) Poliakoff, M.; Weitz, E. *Advances in Organometallic Chemistry*; Stone, F. G. A., Ed.; Academic Press: New York, 1986; Vol. 25, p 277.
(2) Burdett, J. K. *Coord. Chem. Rev.* **1978**, *27*, 1. Hitam, R. B.; Mahmoud, K. A.; Rest, A. J. *Ibid.* **1984**, *55*, 1.
(3) Geoffroy, G. L.; Wrighton, M. S. *Organometallic Photochemistry*; Academic Press: New York, 1979.
(4) Church, S. P.; Hermann, H.; Grevels, F.-W.; Schaffner, K. *J. Chem. Soc., Chem. Commun.* **1984**, 785.
(5) Moore, B. D.; Simpson, M. B.; Poliakoff, M.; Turner, J. J. *J. Chem. Soc., Chem. Commun.* **1984**, 972.
(6) Moore, B. D. Ph.D. Thesis, University of Nottingham, 1985.
(7) Teller, R. G.; Williams, J. M. *Inorg. Chem.* **1980**, *19*, 2778.
(8) Bullitt, J. G.; Cotton, F. A.; Marks, T. J. *J. Am. Chem. Soc.* **1970**, *92*, 2155.
(9) Gansow, O. A.; Burke, A. R.; Vernon, W. D. *J. Am. Chem. Soc.* **1972**, *94*, 2550; **1976**, *98*, 5817.

0002-7863/86/1508-1819$01.50/0